

Anonymous Referee #1

General comments:

- *Overall, the manuscript is well-written, the evaluation methods presented are sound, the manuscript appears to fit reasonably well within the "Model Evaluation" category of GMD, and it presents results that may be of use to future users of MPASv5.2. That said, I have a few significant concerns about the manuscript: it provides minimal discussion about the physical meaning of the results, it lacks discussion of some highly relevant areas of literature, and it lacks a discussion of uncertainty (or statistical significance) in comparisons across resolutions and between simulations and observations. I don't expect that these comments will require much change to the underlying analysis, but I do think they should result in a substantial amount of new or revised text. Based on this, I am recommending that the manuscript be returned to the authors for major revisions*

We thank the reviewer for the detailed and constructive comments. They are very helpful for improving the quality of the manuscript.

In the revised manuscript, we added a new “supporting material” document to include many new figures to support some statements in the text and to address the review comments. We added a discussion of the synoptic condition of this event during the Meiyu front in the introduction. This provides useful information to understand the precipitation differences among the various simulations. Notably, the precipitation biases are related to the shift of circulation pattern in the simulations (Figure S4, S7). In addition, the results of resolution-dependent precipitation and updraft are further discussed in relation to previous studies. Particularly, Fig. 13 on the relationship between precipitation and the upward moisture flux is added to reveal the mechanism of resolution-dependence following Rauscher et al. (2016) and O'Brien et al. (2016). Following the reviewer's suggestion, the bootstrapping statistical analysis is used to test the significance of statistical difference among multiple experiments. Table 2 with the summary of statistical metrics is added with more analysis. Other text and figures have also been revised as the reviewer suggested.

Specific comments:

- *Lack of discussion of physical meaning of results*

Overall, the manuscript reads more like a technical report than a scientific manuscript; it focuses much more on questions of 'what' than questions of 'why'. In my opinion, this severely limits the usefulness of the paper. In its current form, I suspect that the only readers who might find the manuscript interesting would be users of the MPAS-Atmosphere model, since it essentially only focuses on describing how precipitation and vertical velocity characteristics depend on resolution and microphysics. Instead, if the manuscript had a stronger emphasis (even speculative) on why, the manuscript might be of interest to other model users

facing similar questions about the effects of resolution and parameterization.

For example, in Section 3.2.2, the authors present an intriguing result: the GFS model (which are used as initial conditions!) has precipitation that is shifted far too much to the north, whereas the MPAS simulations have the rain band much closer to where it is observed. But the authors provide no speculation on why this might be, nor do they even comment that this is interesting that the MPAS model is able to 'correct' an error in the GFS starting condition. Could it be because of better-resolved topography? Is the northward propagation of the rainband perhaps less rapid in MPAS than in GFS? Are there possibly eddy-mean-flow interactions that MPAS resolves that could cause the rain band to be shifted relative to GFS?

That is just one example; this lack of exploration of 'why' is pervasive in the manuscript. A symptom of this is that almost all of the paragraphs in Section 3 have a fairly repetitive structure in which they (1) introduce a new figure, (2) synthesize information contained in that figure, and (3) report some set of model performance metrics for each run (e.g., spatial correlation coefficients). That said, the authors do explore the effects of resolution on updraft velocity, which does start to get at questions of 'why', but their analysis of this is somewhat superficial, and as discussed in the section below, it misses some key literature that could enrich their analysis and discussion of this.

In summary, the authors should dig quite a bit more deeply in the analysis of their results. I would hope to see mini-hypotheses and hypothesis tests for some of the interesting intra experimental differences that they show.

We thank the reviewer for the suggestion to include more analysis and discussion of the underlying reasons of the differences across multiple experiments. Now we added more analysis and discussion in the manuscript. A new “supporting material” document is added with substantial amounts of figures to explain the model performance. The difference in simulating the precipitation distribution among the experiments is mainly due to the difference in wind shear structure simulated during the Meiyu front of the East Asian summer monsoon. Now more discussion about this is added. For resolution-dependence analysis, Fig. 13 is added to show the relationship between precipitation and upward moisture flux following Rauscher et al. (2016) and O'Brien et al. (2016). The mechanism underlying the simulated resolution-dependent precipitation and updraft is discussed.

Now our discussion of the model results has been substantially enhanced. Here, we list some of the added text in the main manuscript as follows:

“The first precipitation peak was generated by the southwest-northeast wind shear line formed over Central East China along with a vortex over the Southwest at 00 UTC of 26 June. The shear line gradually extended eastward, leading to the second precipitation peak around 00 UTC of 27 June (Fig. S4 in the supporting material). All four experiments generally simulate the Southwest vortex and wind shear during the event,

although the strength and location do not match perfectly with the reanalysis. As the large-scale environment is quite well represented in the model, the simulations also generally capture the two peaks of precipitation along 31°N as observed. However, both U15km and V16km simulate a broader rain belt, resulting in positive biases of precipitation south of 30°N (Fig. S5 in the supporting materials). Both simulations shift the first peak precipitation southward. In addition, the simulations extend the first peak precipitation period and shorten the second one to some extent (Fig. S5). The lower averaged total precipitation around 31°N from the simulation with the NTD parameterization (Fig. 3) is mainly due to the lower rainfall before 26 June compared to the one with the GF parameterization (Fig. S5). For the two precipitation peaks, the simulation with NTD is comparable to the one with GF. Although the two convective parameterizations lead to significant difference in simulating total precipitation before 26 June, both simulations generate consistent wind circulations at 700 hPa before 26 June with spatial correlation coefficients above 0.9 (over the domain as shown in Fig. S4). Although the two convective parameterizations lead to different total precipitation, they have negligible impact on the consistency in modeling precipitation propagation using uniform and variable resolutions during this event.”

“The northward shift of rain belt during the event (shown in Fig. 6 and 7) is related to the GFS forecast that only produced the second peak of precipitation around UTC 0000 of 27 June while totally missing the first peak. In addition, the GFS forecast overestimates the second peak and shift it towards the north by about 4°. The timing and location shift of the rain belt in the GFS forecast are mainly because of the bias in simulating the wind shear in this event. The GFS forecast failed to produce the southwest-northeast wind shear line around UTC 0000 of 26 June, and generated too broad vortex over the west. Around UTC 0000 of 27 June, GFS simulated the wind shear line but locating it further north (Fig. S8 in the supporting material).”

“It is interesting to note that MPAS and GFS forecasts, sharing the same initial condition, simulate different large-scale circulation particularly the wind shear structure with the system evolving (Fig. S8). The model capability in successfully capturing the wind shear structure during this event determines the performance in generating the rain belt evolution. The formation and evolution of wind shear during the Meiyu front over East China have been found interacting with multiscale processes and systems, including terrain and convective latent heat (Yao et al., 2017). Different representation of the terrain over East China in various resolutions may impact the simulated wind shear structure. Previous studies also found that convective latent heat may vary with resolutions and physics (Hagos et al., 2013; Zhao et al., 2016), which can further affect the simulation of wind shear structure. Therefore, the difference in resolution and physics between MPAS and GFS may result in their difference in simulating the formation and evolution of wind shear structure during the event. A more detailed exploration of the differences between the MPAS and GFS simulations is beyond the scope of this study.”

- *Missing discussion of key literature*

The authors devote a significant portion of their analysis and discussion to the connection between vertical velocity and precipitation. This is good, but considering how significant this discussion is to the paper, the authors should discuss how these results relate to a number of recent papers on this connection.

Specifically, there are currently 3 theories in recent literature for why vertical velocity depends on resolution (with the subtext in these manuscripts that these theories can help explain the resolution dependence of precipitation):

*Rauscher, S.A. et al. “A Multimodel Intercomparison of Resolution Effects on Precipitation: Simulations and Theory.” *Climate Dynamics* 47, no. 7–8 (October 27, 2016): 2205–18. doi:10.1007/s00382-015-2959-5.*

*Jeevanjee, N. “Vertical Velocity in the Gray Zone.” *Journal of Advances in Modeling Earth Systems* 9, no. 6 (October 2017): 2304–16. doi:10.1002/2017MS001059.*

*Herrington, A.R., and K.A. Reed. “An Explanation for the Sensitivity of the Mean State of the Community Atmosphere Model to Horizontal Resolution on Aquaplanets.” *Journal of Climate* 30, no. 13 (July 2017): 4781–97. doi:10.1175/JCLI-D-16-0069.1.*

Rauscher et al. suggest that the resolution dependence results from an interaction between the constraint of fluid continuity and macro-scale turbulence. Jeevanjee suggests that the resolution dependence is related to the aspect ratio of ascending parcels, which he argues scales with resolution. Herrington and Reed suggest that the resolution dependence is related to the horizontal-wavelength-dependent growth rate of buoyancy wave instabilities.

At a minimum, this manuscript should discuss these theories, and it would be interesting if the authors provided some sort of analysis that attempts to evaluate these theories in this model. I would also suggest that the authors refer to two other relevant manuscripts: O'Brien et al. (2016) and Fildier et al. (2018), who provide quantitative descriptions of the connection between vertical velocity and extremes (which the authors refer to qualitatively at the end of Section 3).

*O'Brien, T.A. et al. “Resolution Dependence of Precipitation Statistical Fidelity in Hindcast Simulations.” *Journal of Advances in Modeling Earth Systems* 8, no. 2 (June 2016): 976–90. doi:10.1002/2016MS000671.*

*Fildier, B. et al. “Prognostic Power of Extreme Rainfall Scaling Formulas Across Space and Time Scales.” *Journal of Advances in Modeling Earth Systems* 10, no. 12 (2018): 3252–67. doi:10.1029/2018MS001462.*

We thank the reviewer for pointing us to previous studies on the resolution dependence of precipitation simulations. We added more discussion about these studies in the result and discussion parts of the manuscript. We also added Fig. 13 to show the relationship between precipitation and upward moisture flux following previous studies of Rauscher

et al. (2016) and O'Brien et al. (2016). The mechanism underlying the simulated resolution-dependent precipitation and updraft is discussed.

Changes in the text are highlighted as follows:

“Previous studies have proposed some mechanisms underlying the resolution impacts on modeling vertical velocity (e.g., Rauscher et al., 2016; Jeevanjee et al., 2017; Herrington and Reed, 2017; O'Brien et al., 2016; Fildier et al., 2018). Among these mechanisms, Rauscher et al. (2016) argued that the resolution-dependent vertical velocity is caused by the interaction between the constraint of fluid continuity and macro-scale turbulence. They suggested that the vertical velocity should be more intense at higher resolution because the horizontal velocity increment follows approximately a power law of resolution. Therefore, the resolved vertical transport must increase as grid spacing decreases. Assuming atmospheric moisture is relatively insensitive to resolution, the upward moisture flux should increase as grid spacing decreases, hence producing more precipitation.

Figure 13 shows the PDFs of the upward moisture flux and the relationship between hourly precipitation versus upward moisture flux at 850hPa during the event from the MPAS simulations at 60km, 30km, 16km and 4km. It is evident that the simulations at higher resolutions produce more frequent intense upward moisture fluxes at 850hPa, consistent with Rauscher et al. (2016) and O'Brien et al. (2016). Rauscher et al. (2016) found a linear relationship between precipitation and upward moisture fluxes at lower level. The relationship lines from this study as shown in Fig. 13 parallel the 1:1 reference line for all resolutions. However, the lines are consistently below the reference line for convection-permitting simulations (4km) and above the reference line for hydrostatic simulations with convective parameterization (e.g., 16km, 30km, 60km). The simulated precipitation can be larger than the lower level upward moisture fluxes at hydrostatic scale because part of the precipitation is contributed by the convective parameterization rather than contributed by the resolved upward moisture flux (Rauscher et al., 2016). On the contrary, the precipitation could be lower than the upward moisture flux at convection-permitting scale (e.g., 4km) as moisture is removed from the cloud updrafts due to detrainment (e.g., O'Brien et al., 2016). Overall, our results of the resolution-dependent updraft and precipitation are consistent with Rauscher et al. (2016) and O'Brien et al. (2016).”

“Previous studies (Xue et al., 2007; Clark et al.) noted the importance of ensemble simulations in predicting heavy precipitation. Due to computational limitation, only one set of experiments with different physics and resolutions are evaluated in this study. The MPAS simulations of heavy precipitation with different initial conditions and refinement sizes deserve more evaluations. Finally, some studies noted that convection-permitting modeling does not always add values in simulating heavy precipitation compared to hydrostatic scale modeling (e.g., Kain et al., 2008; Rhoades et al., 2018; Xu et al., 2018). Rhoades et al. (2018) found that the improvement by increasing resolution may depend

on cloud microphysics parameterization. Increasing horizontal resolution alone sometimes can even lead to worse model performance. The impacts of increasing horizontal resolution on the overall model performance in simulating extreme precipitation may also be affected by the model structure and coupling among model components and processes (Jeevanjee et al., 2016; O'Brien et al., 2016; Herrington et al., 2017, 2018; Gross et al., 2018). This study also found some sensitivity of modeling extreme precipitation to cloud microphysics, particularly at convection-permitting scale."

- ***Lack of statistics***

The authors make a variety of quantitative statements comparing across simulations or between simulations and observations: e.g., "As a result, the correlation coefficients between the observations and the MPAS experiments at the resolutions of 60 km, 30 km, 16 km, and 4 km are 0.20, 0.21, 0.29, 0.50 (WSM6), and 0.42 (Thompson), respectively" (lines 422-424). However, the authors do not provide any estimates of uncertainty in these quantities, which makes it difficult to assess whether they are significant. I would expect that many of them are, but if a core goal of this paper is to assess how model skill changes with resolution, the authors should be certain that their claims are statistically robust. I see two straight-forward ways to assess uncertainty: bootstrap confidence intervals (e.g., bootstrap sample from spatial points), or running ensembles. Ideally, the authors would run more ensemble members, but I recognize that computational constraints may prohibit that. At the very least, a bootstrap analysis would allow the authors to state the sampling uncertainty in the correlation coefficients.

Related to this, it does concern me that all of the conclusions in this manuscript are based on single-member ensembles of a single event. Would these results hold if the authors simulated another event, perhaps in another season, or even if the authors ran another ensemble member? The authors should at very least acknowledge this limitation of their study, and at best run a few additional simulations to explore whether new simulations qualitatively alter their conclusions.

We thank the reviewer for the suggestion to test the statistical significance. Due to the large computing cost and data storage, particularly for the U15km and V4km experiments, we cannot afford to perform ensemble simulations in this study. Instead, we take the suggestion by the reviewer to use the bootstrap sampling method to test the statistical significance. The statistical test confirms that the difference among the experiments is statistically significant. We added Table 2 with the summary of statistical metrics and more analysis in the revised manuscript. The conclusion of this study does not change. Now we acknowledge this in the method as follows:

"Due to the large computing cost and data storage of the experiments conducted, particularly for the U15km and V4km experiments, this study does not perform ensemble simulations. Instead, the bootstrapping statistical analysis is used to test the statistical

significance of the difference among multiple experiments investigated in this study. The bootstrap method uses resampling technique to extract certain samples, called bootstrap samples, within the range of the original data. Statistical metrics such as averages, variances, correlation coefficient, can be calculated for each bootstrap sample. For a given confidence level (e.g., 95%), bootstrap confidence intervals of specific statistical metric can be estimated (e.g., Efron, 1992; Efron and Tibshirani, 1994).”

We added Table 2 to summarize the statistical metrics and more discussion about the statistical significant tests with the bootstrap method has been added in the text:

“In order to test the statistical significance of the difference among the experiments, the 95% confidence intervals of spatial correlation are estimated based on the bootstrap analysis. Although the correlation coefficients estimated above have an uncertain range, at the 95% confidence level the results still indicate that the V16km simulation produces better spatial pattern of precipitation than other hydrostatic-scale simulations. In addition, the simulation at the convection-permitting scale is comparable to, if not better than, the V16km simulation. The results are summarized in Table 2.”

“At the 95% confidence level (Table 2), the experiments at 16 km and 4 km are comparable in terms of simulating the propagation of the rain belt and better than the experiments at other resolutions.”

“The statistical significance tests based on the bootstrap analysis indicate that at the 95% confidence level the model performance at 16 km and 4 km in terms of simulating vertical structure of winds are comparable and better than the simulations at coarser resolution (Table 2).”

“The statistical significance tests based on the bootstrap analysis indicate that at the 95% confidence level the model performance at 16 km and 4 km in terms of simulating vertical structure of winds are comparable and better than the simulations at coarser resolution (Table 2).”

“The statistical significance test based on the bootstrap analysis indicates that at the 95% confidence level the simulations at 4 km can better capture the spatial distribution of heavy precipitation than the simulations at resolutions of hydrostatic scale (Table 2).”

This study focuses on evaluating the MPAS simulations of heavy precipitation over East China (Yangtze River Delta Region). Most of heavy precipitation events over East China occurred in summer, so we focused on the events in summer instead of other seasons. The event we selected in this study was reported as one of the most influential precipitation events in summer of 2012 over East China. See our response to your other comments about the reason selecting this event.

Due to the computational limitation, we only run one set of experiments with different physics and resolutions. We agree that it may not represent all the cases. We acknowledge that one case study is not enough to fully evaluate the MPAS performance

over East China. Now, we added the discussion in the summary section:

“Due to the computational limitation, only one set of experiments with different physics and resolutions are evaluated. The MPAS simulations of heavy precipitation over East China with different initial conditions and refinement sizes deserve more evaluations.”

“more events of heavy precipitation over East China should be investigated in the future to more systematically evaluate the MPAS variable-resolution modeling framework and the impacts of resolution and physical parameterizations.”

- *lines 100-101: "regional models limit feedback to global scale". This is true, but is that really a good point to make in this paper? The simulations only run for ~5 days, so there is very little time for feedback--e.g., from rossby wave propagation--to feedback onto global scales. In my opinion, that makes this point a bit irrelevant, and almost misleading for this paper, since it could be read to imply that this gives these variable-resolution simulations an advantage in this experimental design over limited-area model approaches.*

Thanks for this suggestion. Since this study is about forecasting of an extreme event, the feedback we care about is the feedback that would affect the forecasting of the extreme precipitation event. In this context, the feedback is through condensational heating that generates potential vorticity and excites Rossby waves that influence the storm. 5-day is long enough to see the impacts of the storm on mesoscale and large-scale circulation that influence the storm. Now we correct the sentence in the text as “...and also limit regional feedback to large-scale circulation”.

- *lines 129-131: Why were these dates chosen? Presumably it is because it is a representative, strong event; or perhaps it was chosen randomly. But a cynical version of that answer could be 'because it was a date for which the model looked very good'--I truly doubt this is case, but without any discussion of the motivation for choosing this date, a reader could wonder if this date was cherry-picked.*

This study focuses on evaluating the MPAS simulations of heavy precipitation over East China (Yangtze River Delta Region). Most of heavy precipitation events over East China occurred in summer. The event we selected in this study was reported as one of the most influential precipitation events in summer of 2012 over East China. We agree that a single event may not represent all the cases. As we respond to one comment above, we acknowledge that one case study is not enough for fully evaluating the MPAS performance over East China. Now, we added the clarification in the introduction section as “A heavy precipitation event that occurred on June 25-27 of 2012 over the YRD of East China, one of the ten heaviest precipitation events in 2012, is selected. This rainfall event was triggered by a typical southwest vortex in the middle and high troposphere and wind shear in the lower layer of Meiyu front over East China during the East Asian summer monsoon (e.g., Xiang et al., 2013; Yao et al., 2017), initiated around 1200 UTC of 25 June. During this period, a heavy precipitating system propagated along the Yangtze River and produced as much as 244 mm of precipitation in 24 hours at some

locations. The continuous precipitation led to 17 deaths and about RMB 3.68 billion in total damage, and affected more than 685 million people in the provinces of Central and East China.”

We added the discussion in the summary section:

“Due to the computational limitation, only one set of experiments with different physics and resolutions are evaluated. The MPAS simulations of heavy precipitation over East China with different initial conditions and refinement sizes deserve more evaluations.”

“more events of heavy precipitation over East China should be investigated in the future to more systematically evaluate the MPAS variable-resolution modeling framework and the impacts of resolution and physical parameterizations.”

- *lines 235-241: The authors provide very little discussion on the meteorological conditions preceding the event, or of the initial condition. This limits the author's and the reader's ability to interpret differences between the simulations and observations. For example, was the Meiyu front already present and propagating in the initial condition, or did it form in the day or two preceding (presumably it was already present)?*

The event studied occurred mainly on June 25-27. This event was triggered by a typical southwest vortex in the middle and high troposphere and wind shear in the lower layer of Meiyu front over East China during the East Asian summer monsoon. The wind shear structure formed on June 25. The simulation started on June 23. Therefore, the wind shear structure is not present in the initial condition. More discussion about the synoptic condition of this event is added in the text:

“A heavy precipitation event that occurred on June 25-27 of 2012 over the YRD of East China, one of the ten heaviest precipitation events in 2012, is selected. This rainfall event was triggered by a typical southwest vortex in the middle and high troposphere and wind shear in the lower layer of the Meiyu front over East China during the East Asian summer monsoon (e.g., Xiang et al., 2013; Yao et al., 2017), initiated around 1200 UTC of 25 June. During this period, a heavy precipitating system propagated along the Yangtze River and produced as much as 244 mm of precipitation in 24 hours at some locations. The continuous precipitation led to 17 deaths and about RMB 3.68 billion in total damage, and affected more than 685 million people in the provinces of Central and East China.”

We added the discussion about the formation and evolution of the system:

“The first precipitation peak was generated by the southwest-northeast wind shear line formed over Central East China along with a vortex over the Southwest at 00 UTC of 26 June. The shear line gradually extended eastward, which led to the second precipitation peak around 00 UTC of 27 June (Fig. S4 in the supporting material).”

- *line 246: The authors should use ERA5 instead. It covers this date, it has a significantly higher resolution, and the data are very easy to obtain either directly from ECMWF or from the NCAR RDA.*

Thanks for your suggestion. Now we change the reanalysis data from ERA-interim to ERA5 in the figures and revise the related discussion. The results and conclusion are similar.

Anonymous Referee #2

General comments:

- *Zhao et al. in “Modeling extreme precipitation over East China with a global variable resolution modeling framework (MPASv5.2) Impacts of resolution and physics” recreate an extreme weather event that occurred over East Asia between 25-27 June 2012. This study presents a comprehensive look at the performance of the Model for Prediction Across Scales (MPAS) across both hydrostatic and non-hydrostatic scales (e.g., 60km to 4km), uniform and variable-resolution grid-spacing, and three different microphysics schemes (one of which is “scale aware” for convective/resolved precipitation). The authors assess MPAS skill compared with CMA observations in East Asia and tersely compare results to GFS forecasts over a single-member, sub-weekly simulation period.*

Overall, I think the paper is well written and fits within the scope of GMD and could be, given a bit more work, a valuable contribution to the scientific community, particularly due to its emphasis on evaluating the use new variable-resolution global climate models for extreme event recreation and sub-weekly weather forecasting. However, I think there are still several major revisions that need to happen prior to this paper being accepted. I would suggest that the editor assign major revisions to this manuscript.

We thank the reviewer for the detailed review. The comments help a lot on improving the quality of the manuscript.

In the revised manuscript, we provided a more nuanced assessment of simulations. The difference between observations and simulations are highlighted to provide a more balanced discussion of model skill. Due to the large amounts of experiments conducted in this study, the computational and storage demands are very large, preventing the ensemble simulations. Following the other reviewer’s suggestion, the bootstrapping statistical analysis is used to test the statistical significance of the difference among multiple experiments. The statistical metrics are now summarized in Table 2 in the revised manuscript. In terms of resolution-dependence analysis, more discussion about previous related studies are also added. Other text and figures have also been revised as the reviewer suggested. A new document on supporting material is added in the revised manuscript with substantial amounts of figures to support some statements and address the comments.

Major comments:

- *1) Given that this paper centers around the recreation of one weather event, why did the authors not perform an ensemble of simulations with slightly perturbed initial conditions to highlight internal variability impacts on precipitation intensity and spatial distribution? Was the computational demand too high to do so? If so, as mentioned below, it would benefit the reader to know this type of information*

explicitly. If not, why not perform, at least, a small ensemble of simulations (as the authors state is needed for GFS in Section 4 – line 529).

a) Line 213-215 – This might be a good time to bring up real-time computational demand (e.g., nodes used, simulated years per actual day, etc.) and physics/dynamics timesteps across “U” and “V” cases.

Due to the large amounts of experiments conducted in this study, the computational and storage demands are very large, preventing the ensemble simulations. Instead, the bootstrapping statistical analysis is used to test the significance of statistical difference among multiple experiments investigated in this study. Now it is clarified in the text “Due to the large computing cost and data storage of the experiments conducted, particularly for the U15km and V4km experiments, this study does not perform ensemble simulations. Instead, the bootstrapping statistical analysis is used to test the significance of statistical difference among multiple experiments investigated in this study.”

Now we also added more information about the configurations of multiple experiments in the text:

“The difference in the number of mesh cells leads to a difference in computational and storage demand. With the TH-2 supercomputer of National Supercomputer Center in Guangzhou (NSCC-GZ), it takes ~9000 CPU hours and ~240 CPU hours to finish one-day simulation for U15km and V16km resolutions, respectively. In addition, with the standard MPASv5.2, the sizes of output data per one-day simulation for U15km and V16km are 0.5 T and 0.02 T, respectively. The same time step of 60 second is used for physics and dynamics for both U15km and V16km simulations.”

“The numbers of grid cells in the U60km, V30km, V16km, and V4km meshes are ~0.16 million, 0.10 million, ~0.11 million, and ~0.8 million, respectively. Difference in the number of cells and minimum cell size also leads to the difference in computational and storage demand. With the TH-2 supercomputer of NSCC-GZ, it takes ~200 CPU hours, ~150 CPU hours, ~240 CPU hours, and ~1800 CPU hours to finish one-day simulation for U60km, V30km, V16km, and V4km meshes, respectively. In addition, with the standard MPASv5.2, the sizes of output data per one-day simulation for the four meshes are 0.03 T, 0.02 T, 0.02 T, and 0.15 T, respectively. The time steps used for physics and dynamics for the four meshes are 300 seconds, 120 seconds, 60 seconds, and 20 seconds, respectively.”

- *2) The authors should highlight other variable-resolution modeling efforts to give readers a sense that there are a community of models now available.*
 - a) Line 106 – Given that the authors examine both hydrostatic and non-hydrostatic configurations of MPAS, the authors should also point to the literature of hydrostatic variable-resolution global climate models such as variable-resolution CESM (etc.) as these variable-resolution options have been used extensively for*

various applications (e.g., Rauscher et al., 2013; Zarzycki et al., 2014, 2015; Rhoades et al., 2016; Huang et al., 2016; Wu et al., 2017; Gettelman, et al., 2018; Wang et al., 2018; Burakowski et al., 2019).

Although this study investigated some MPAS simulations at the hydrostatic scales, the MPAS model used in all the experiments in this study is the fully compressible non-hydrostatic version (MPAS-A v5.2) as described in the manuscript. We did not examine the hydrostatic configurations of MPAS. However, we thank the reviewer for pointing out previous literatures using other variable-resolution models such as CESM. Now these previous studies are mentioned and the literatures are cited in the text “*Although global hydrostatic variable-resolution climate models, such as the variable-resolution version of Community Earth System Model, have been used extensively for various applications (e.g., Rauscher et al., 2013; Zarzycki et al., 2014, 2015; Rhoades et al., 2016; Huang et al., 2016; Wu et al., 2017; Gettelman, et al., 2018; Wang et al., 2018; Burakowski et al., 2019), so far few studies used global non-hydrostatic variable-resolution models to investigate weather or climate simulations, particularly at convection-permitting scales (e.g., Prein et al., 2015).*”

- *3) This manuscript would also benefit from the discussion of previous studies that have shown that solely refining horizontal resolution alone has led to differing results in simulated precipitation bias across various models (including variable-resolution approaches).*
 - a) Line 83-87 – There also have been studies showing that solely refining horizontal resolution alone can lead to unexpected “oscillations” between positive/negative simulated bias in daily-to-seasonal average precipitation too. For example, refining horizontal resolution from 55km to 28km has been shown to improve various assessments of simulated bias (e.g., orographic precipitation, hurricanes, atmospheric rivers, etc.), however refining resolution from 28km to 14km has shown an enhancement of bias (Rhoades et al., 2018; Xu et al., 2018). These differences have been shown to be bounded in theory and model structure decisions (Jeevanjee et al., 2016; O’Brien et al., 2016; Herrington et al., 2017, 2018; Gross et al., 2018). The authors should discuss these studies as well to give the readers clear perspective that resolution alone will not be the sole solution to better representations of extreme precipitation.*

Thanks for the reviewer in pointing out the interesting and related studies. We agree that resolution alone will not always improve the simulations. Now we added more discussion about previous studies to highlight the resolution impacts. We clarified in the text in the introduction:

“Although not a panacea for weather and climate modeling (NRC, 2012), previous studies suggested that increasing grid resolution could significantly improve modeling of extreme precipitation because the impacts of topography, land-use, land-atmosphere

interaction, and other important processes are better resolved (e.g., Giorgi and Mearns, 1991; Giorgi and Marinucci, 1996; Leung et al., 2003; Bacmeister et al. 2014; ECMWF2016).”

We added the text in the discussion:

“Finally, some studies noted that convection-permitting modeling does not always add values in simulating heavy precipitation compared to hydrostatic scale modeling (e.g., Kain et al., 2008; Rhoades et al., 2018; Xu et al., 2018). Rhoades et al. (2018) found that the improvement by increasing resolution may also depend on cloud microphysics parameterization. Increasing horizontal resolution alone sometimes can even lead to worse model performance. The impacts of increasing horizontal resolution on the overall model performance in simulating extreme precipitation may also be affected by the model structure and coupling among model components and processes (Jeevanjee et al., 2016; O’Brien et al., 2016; Herrington et al., 2017, 2018; Gross et al., 2018). More events of heavy precipitation over East China should be investigated in the future to more systematically evaluate the MPAS variable-resolution modeling framework and the impacts of resolution and physical parameterizations.”

b) Figure 4 and 8 – These two plots somewhat prove the point made above that if CMA is used as the simulation skill benchmark and by eye, another reason Figure 4 and 8 should be difference plots, V16km seems to get the timing of the two locations of precipitation maxima and magnitudes the most correct over the storm track (i.e., 30 N +/-2 deg), whereas at V4km the precipitation magnitudes seem too positively biased over a greater area and longer time. I think these plots also highlight the potential need for an ensemble of simulations given that the time-space structure of precipitation in each of the simulations is quite different and could simply be due to using one realization of the atmospheric internal variability.

Thanks for your comment, and we agree that the simulated timing and magnitudes do not perfectly match the observations. We show the simulated temporal-spatial distribution of precipitation instead of the difference against the observation, because in this way the simulated propagation of rain belt can be better demonstrated although there are biases. From both Fig. 4 and 8, we can see clearly some simulations can capture the propagation better than others, particularly for V16km.WSM6 and V4km.WSM6. Now we added Fig. S5 and Fig. S9 in the supporting materials to show the difference between the simulations and observations. We also added more discussion about the difference in the text:

“All four experiments generally simulate the southwest vortex and wind shear during the event, although the strength and location do not match perfectly with the reanalysis. As the large-scale environment is quite well represented in the model, the simulations also generally capture the two peaks of precipitation along 31°N as observed. However, both U15km and V16km simulate a broader rain belt, resulting in positive biases of

precipitation south of 30°N (Fig. S5 in the supporting materials). Both simulations shift the first peak precipitation southward. In addition, the simulations extend the first peak precipitation period and shorten the second one to some extent (Fig. S5 in the supporting materials). The lower averaged total precipitation around 31°N from the simulation with the NTD parameterization (Fig. 3) is mainly due to the lower rainfall before 26 June compared to the one with the GF parameterization (Fig. S5). For the two precipitation peaks, the simulation with NTD is comparable to the one with GF. Although the two convective parameterizations lead to significant difference in simulating total precipitation before 26 June, both simulations generate consistent wind circulations at 700 hPa before 26 June with spatial correlation coefficients above 0.9 (over the domain as shown in Fig. S4 in the supporting material). Although the two convective parameterizations lead to different total precipitation, they have negligible impact on the consistency in modeling precipitation propagation using uniform and variable resolutions during this event.”

“The northward shift of rain belt during the event (shown in Fig. 6 and 7) is related to the GFS forecast that only produced the second peak of precipitation around UTC 0000 of 27 June while totally missing the first peak. In addition, the GFS forecast overestimates the second peak and shift it towards the north by about 4°. The timing and location shift of the rain belt in the GFS forecast are mainly because of the bias of GFS in simulating the wind shear in this event. The GFS forecast failed to produce the southwest-northeast wind shear line around UTC 0000 of 26 June and generated too broad vortex over the west. Around UTC 0000 of 27 June, GFS simulated the wind shear line but locating it further north (Fig. S8 in the supporting material).”

“All simulations roughly produce the two peaks of precipitation as observed during the event. However, the experiment at 60 km simulates the first precipitation peak southward and the second peak northward of the observations, while the experiment at 30 km simulates the second peak further south and a few hours earlier. The time and location shift corresponding well to biases in simulated wind shear (Fig. S8). The spatial correlation coefficients of precipitation are 0.30 and 0.32 between the observations and the simulations at 60 km and 30 km, respectively. The experiments at 16 km and 4 km with the WSM6 cloud microphysics scheme can better capture the timing and latitude of the observed precipitation event than U60km and V30km (Fig. S9 in the supporting materials), however both V16km and V4km overestimate the first peak precipitation and underestimate the second peak. The experiment at 4 km with the Thompson scheme overestimates the precipitation amount of both peaks.”

In terms of ensemble simulations, due to the large amounts of experiments conducted in this study, the computational and storage demands are very large. Instead, the bootstrapping statistical analysis is now added to test the significance of statistical difference among multiple experiments investigated in this study. Table 2 is added to

summarize the statistical analysis. Now it is also clarified in the text “Due to the large computing cost and data storage of the experiments conducted, particularly for the U15km and V4km experiments, this study does not perform ensemble simulations. Instead, the bootstrapping statistical analysis is used to test the significance of statistical difference among multiple experiments investigated in this study.”

- *4) Given the emphasis on microphysics choice (e.g., three different ones used in this manuscript), a more in-depth discussion of each of the microphysics schemes should be presented in Section 2. In my opinion, the reader should be able to glean some of the tradeoffs of each of the microphysics schemes within the text and not just be referred to other publications.*

a) Line 186 – Highlight a bit more detail about the microphysics schemes used as they can impact the spatial distribution of extreme precipitation that you discuss later on. For example, one-moment vs two-moment schemes, diagnostic vs prognostic, which hydrometeor species are represented in each scheme (i.e., rain, snow, graupel, etc.), what are their assumptions in drop velocity, horizontal advection, etc. A new book chapter has been published that could be a good lead on this as well (Gettelman et al., 2019).

Thanks for your suggestion. This study used two cloud microphysics schemes available in MPAS, i.e., WSM6 and Thompson. Now more details about the two schemes are added in Section 2 as “For cloud microphysics, the WSM6 (Hong and Lim, 2006) and Thompson (Thompson et al., 2008) schemes, both of which are bulk microphysical parameterizations, are selected. Both schemes include six hydrometeor species: water vapor, cloud water, rain, cloud ice, snow, and graupel. The WSM6 scheme is a one-moment prognostic parameterization, while the Thompson scheme includes a two-moment prognostic parameterization for cloud ice and the single-moment parameterization for the other hydrometeor species. The two schemes apply the same formula of gamma distribution of hydrometeor species: $N(D) = N_0 D^\mu e^{-\lambda D}$, where D is the particle diameter, N_0 is the intercept parameter, μ is the shape factor, and λ is the slope parameter, although the parameter values or functions vary in the two schemes. The mass-size relationship in WSM6 and Thompson is also expressed in the same formula as $m(D) = aD^b$. The mean falling speed is calculated as $V(D) = cD^d (\frac{\rho_0}{\rho})^{0.5}$ in WSM6 and $V(D) = cD^d (\frac{\rho_0}{\rho})^{0.5} \exp(-fD)$ in Thompson, respectively (Hong and Lim, 2006; Thompson et al., 2008). In the formula, the WSM6 scheme assumes a power-law fit between terminal velocity and particle size as Locatelli and Hobbs (1974), while the Thompson scheme incorporates an exponential decay parameter to allow for a decrease in falling speed with increasing size (Molthan et al., 2012).”

- *5) The authors could give a more nuanced assessment of MPAS skill. Based on*

how the text has been written, MPAS never seems to perform poorly, yet correlation coefficients and spatial structures of the storm events in the figures clearly show important differences compared with observations. In addition, the authors should be very clear over which area the correlation coefficients are being computed given that they are used throughout the text. I presume these correlations are computed over the entire domain. Given that this study is evaluating performance over a single weather event, shouldn't the correlation coefficients be computed over the "mean" track of the event (i.e., using CMA as reference, 30 N +/- 2 deg lat)

Now we added more discussion about the difference between the observations and MPAS results, particularly for Fig. 4 and 8 ([see our response to your other comments](#)). We added clarification in the text to indicate that the spatial correlation coefficients were calculated for the entire regions shown in the specific figures. Besides the entire region of East China, we did evaluate the performance over the rain belt region (27°N-32°N and 110°E-122°E) as shown in Fig. 10 and include the discussion in Section 3.2.3.

- a) *Shouldn't ERA5 rather than GFS be used for forecast comparison skill? ERA5 resolution is much more closely aligned with MPAS horizontal resolutions used in this study.*

The publicly available ERA5 forecast is only for 18-hour, so it cannot be used as the reference to compare with the 5-day MPAS forecast starting from 0000 UTC of 23 June 2012. However, now we changed the reanalysis data from ERA-interim to ERA5 in all the related figures and analysis.

- b) *Line 289-290 – A correlation coefficient of 0.48 and 0.42 for the GF scheme simulations doesn't indicate to me that these simulations reproduce the observed precipitation propagation. I agree with your later assessment that the differences between "U" and "V" simulations are small, especially for NTD, (which is an interesting result), but to say this compares well with observed is a bit misleading. I think this statement (and others like it) must be a bit more caveated and highlight the negatives/positives of the simulations more clearly.*

In the revised manuscript, now we provided a more nuanced assessment of simulations. Now more discussion about the difference between the observations and simulations are added as ["All four simulations show that the rain belt started from the South and eventually stayed around 31°N. The simulations also generally show the two peaks of precipitation along 31°N as observed. However, both U15km and V16km simulate broader rain belt, resulting in positive biases of precipitation south of 30°N \(Fig. S5 in the supporting materials\). Both simulations shift the first peak precipitation southward. In addition, the simulations extend the first peak precipitation period and shorten the second one to some extent \(Fig. S5 in the supporting materials\)."](#) Now Fig. S4 is also added in the supporting materials to show the difference between the observations and simulations.

- c) *Figure 8 – This plot (as indicated below) should be remade into a difference plot. If one uses CMA as reference, it appears that the precipitation maxima during this event occurs too soon (i.e., one-day) across all of the simulations.*

Thanks for your comment, and we agree that the simulated timing and magnitudes do not perfectly match the observations. See our response to your comment above. Now we added Fig. S9 in the supporting materials to show the difference between the simulations and observations. We also added more discussion about the difference shown in Fig. 8 and Fig. S9 in the text:

“The northward shift of rain belt during the event (shown in Fig. 6 and 7) is related to the GFS forecast that only produced the second peak of precipitation around UTC 0000 of 27 June while totally missing the first peak. In addition, the GFS forecast overestimates the second peak and shift it towards the north by about 4°. The timing and location shift of the rain belt in the GFS forecast are mainly because of the bias of GFS in simulating the wind shear in this event. The GFS forecast failed to produce the southwest-northeast wind shear line around UTC 0000 of 26 June and generated too broad vortex over the west. Around UTC 0000 of 27 June, GFS simulated the wind shear line but locating it further north (Fig. S8 in the supporting material).”

“All simulations roughly produce the two peaks of precipitation as observed during the event. However, the experiment at 60 km simulates the first precipitation peak southward and the second peak northward of the observations, while the experiment at 30 km simulates the second peak further south and a few hours earlier. The time and location shift corresponding well to biases in simulated wind shear (Fig. S8). The spatial correlation coefficients of precipitation are 0.30 and 0.32 between the observations and the simulations at 60 km and 30 km, respectively. The experiments at 16 km and 4 km with the WSM6 cloud microphysics scheme can better capture the timing and latitude of the observed precipitation event than U60km and V30km (Fig. S9 in the supporting materials), however both V16km and V4km overestimate the first peak precipitation and underestimate the second peak. The experiment at 4 km with the Thompson scheme overestimates the precipitation amount of both peaks.”

Minor comments:

- *Line 217-221 – The authors may want to include this analysis of minimal precipitation difference in the supplemental for reader clarification.*

Now we added the figures in the supplemental materials showing the total and resolved precipitation from the V16km simulations with both WSM6 and Thompson cloud microphysics. We also added clarification in the text as “The impact of cloud microphysics (WSM6 and Thompson) on the consistency in modeling total precipitation is also examined and is found to be negligible (Fig. S1 and S2 in the supporting materials), although there are some impacts on the simulated grid-resolved precipitation

(Fig. S3 in the supporting materials).”

- *Line 238 – In MPAS, could reanalysis data also be used to replace the coarse resolution portion of the simulation outside of the refinement regions (i.e., akin to a conventional regional climate model)? This could be an interesting next step for a future publication (unless it has already been done) to limit model drift due to the large-scale boundary conditions.*

This is a good point. It deserves effort in future, but this capability is not in the current released version of MPAS.

- *Line 263 – Given that you point to the Meiyu front a few times in this text, you may want to spend a bit of time in the introduction to discuss the importance of the Meiyu front for shaping East Asian precipitation and cite some studies for further reading.*

Thanks for your comment. Now more discussion about the synoptic condition of this event is added in the introduction as “A heavy precipitation event that occurred on June 25-27 of 2012 over the YRD of East China, one of the ten heaviest precipitation events in 2012, is selected. This rainfall event was triggered by a typical southwest vortex in the middle and high troposphere and wind shear in the lower layer of Meiyu front over East China during the East Asian summer monsoon (e.g., Xiang et al., 2013; Yao et al., 2017), initiated around 1200 UTC of 25 June. During this period, a heavy precipitating system propagated along the Yangtze River and produced as much as 244 mm of precipitation in 24 hours at some locations. The continuous precipitation led to 17 deaths and about RMB 3.68 billion of total damage, and affected more than 685 million people in the provinces of Central and East China.”

- *Line 283-284 – Again, the authors may want to offer this analysis in the supplemental material to allow for readers to determine how “negligible” the results were between microphysics schemes.*

Now, we added the figures in the supplemental materials showing the total and resolved precipitation from the V16km simulations with both WSM6 and Thompson cloud microphysics. We also added clarification in the text as “The impact of cloud microphysics (WSM6 and Thompson) on the consistency in modeling total precipitation is also examined and is found to be negligible (Fig. S1 and S2 in the supporting materials), although there are some impacts on the simulated grid-resolved precipitation (Fig. S3 in the supporting materials).”

- *Line 324 – I think the authors should guide the readers intuition on GFS skill at 1 deg and 0.5 deg (seems pretty poor compared with CMA) as a comparison to MPAS. This seems to be a central point of the study that MPAS can offer enhanced*

skill (in some measures) for extreme precipitation forecasts, but seems to be a bit muted in the text. Line 341 – Again, the authors may want to put this analysis that is not shown in the supplemental.

As we mentioned in the manuscript “Since the focus of this study is not to investigate the difference between MPAS and GFS and to evaluate the performance of GFS, details about the GFS are not discussed here but can be found on the website listed above.”, we do not want to guide the readers about the performance of GFS. The GFS product is only used as a reference in this study, and the central point of this study is evaluating the MPAS performance against observations. Now the comparison of global distributions is put in the supporting material.

- *Line 355 – What does “fairly well” indicate? This is an example of the larger major comment that MPAS skill is not evaluated in a nuanced fashion.*

Thanks for your suggestion. “fairly well” is deleted now.

- *Line 366-368 – If I’m reading the space-time plots correctly, it appears that the peak precipitation of the weather event at 30 N +/- 2 deg consistently occurs a day earlier than expected compared with CMA (save for V4km.Thompson which seems to overly precipitate over several days). Therefore, if this is true, the use of the word “roughly similar” is a bit misleading.*

“roughly the same time” is deleted. Now we added more discussion about the difference between the observations and simulations. [See our response to your other comments.](#)

- *Line 489-490 – Another example of a slightly misleading statement about the MPAS 4km simulation skill. The heavy precipitation is captured much better than other coarser resolution MPAS simulations, but precipitation magnitudes, especially maxima, are high biased and precipitation durations are biased over a much longer time than other resolutions (e.g., Figure 8). In my opinion, this warrants a Table that explicitly states the summary statistics for each of the MPAS simulations (and CMA as well).*

Now we revised the statement and added more discussion in the text as “Among the MPAS experiments with multiple resolutions, the simulations at 4 km can better capture the observed locations of heavy precipitation than the ones at hydrostatic scales, however, the results also show that the simulations at 4 km overestimate the first peak precipitation and underestimate the second one. The simulations at 4 km are also very sensitive to cloud microphysics, which deserves more investigation in future.” Table 2 is also added to summarize the statistics among the multiple experiments.

- *Figure 2 – The authors may want to make the color labels from 0-1 mm/day white instead of blue. This might make it easier to see the vector winds.*

Revised. Thanks for your suggestion.

- ***Figure 4 and 8 – Given that these plots are meant to just show the spatial distribution of precipitation (and not include vector winds) compared with the observed CMA product, the authors may want to provide these plots as difference plots to help readers locate mismatch. This would also highlight how GFS is suboptimal for forecasting extreme precipitation events in East Asia at the moment. Also, in Figure 8, each title should be consistent with the explicit use of WSM6 or Thompson microphysics.***

Now the difference plots are added as Fig. S5 and Fig. S9 in the supporting materials. More discussion is also added. See our response to your other comments. The titles of Fig. 8 are changed as suggested.

- ***Figure 5 – Given that this plot is purely meant to show the partitioning of resolved and parameterized precipitation across resolutions spanning hydrostatic/non-hydrostatic scales, could the authors change the units from mm/day and instead use a % of total precipitation? Again, I would suggest that a white/transparent color be used at the lower end of the color bar as well.***

The fraction plot will show large values over the small total precipitation region and make the result misleading. Now we revised Fig. 5 to adjust the colorbar and added Fig. S6 in the supporting material to show the fraction of resolved and parameterized rain in the total. We also added discussion in the text as “**The fraction of parameterized precipitation in the total decreases significantly from the simulations at 16 km to the ones at 4km over the heavy precipitation region (Fig. S6 in the supporting materials). It is also interesting that the fraction of parameterized precipitation increases from the simulations at 60 km to the ones at 16 km to some extent.**”

- ***Figure 6 – I would suggest that a white/transparent color be used at the lower end of the color bar to focus reader attention and more clearly present vector winds.***

Revised. Thanks for your suggestion.

- ***Table 1 – The table should be standalone; therefore, “U” and “V” should be defined in the caption (i.e., Uniform and Variable Resolution) and WSM6, NTD, GF, etc. should be as well.***

Thanks for your suggestion. Now the note is added with the table.

Supporting materials for “Modeling extreme precipitation over East China with a global variable-resolution modeling framework (MPASv5.2): Impacts of resolution and physics”

¹Chun Zhao, ¹Mingyue Xu, ¹Yu Wang*, ¹Meixin Zhang, ²Jianping Guo, ³Zhiyuan Hu, ⁴L. Ruby Leung, ⁵Michael Duda, ⁵William Skamarock

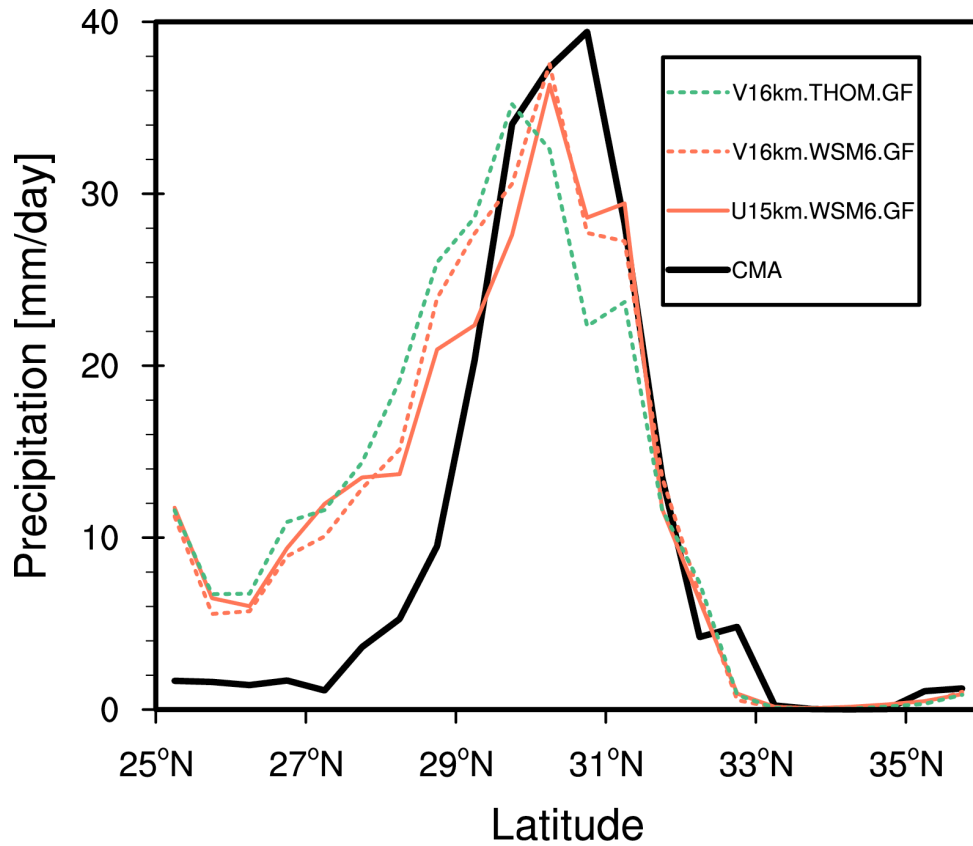
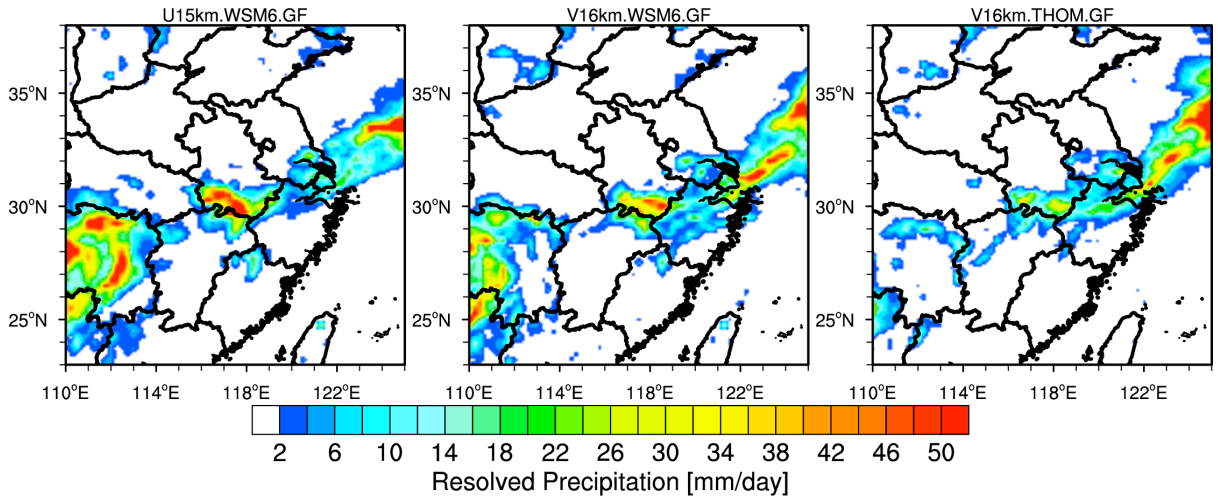
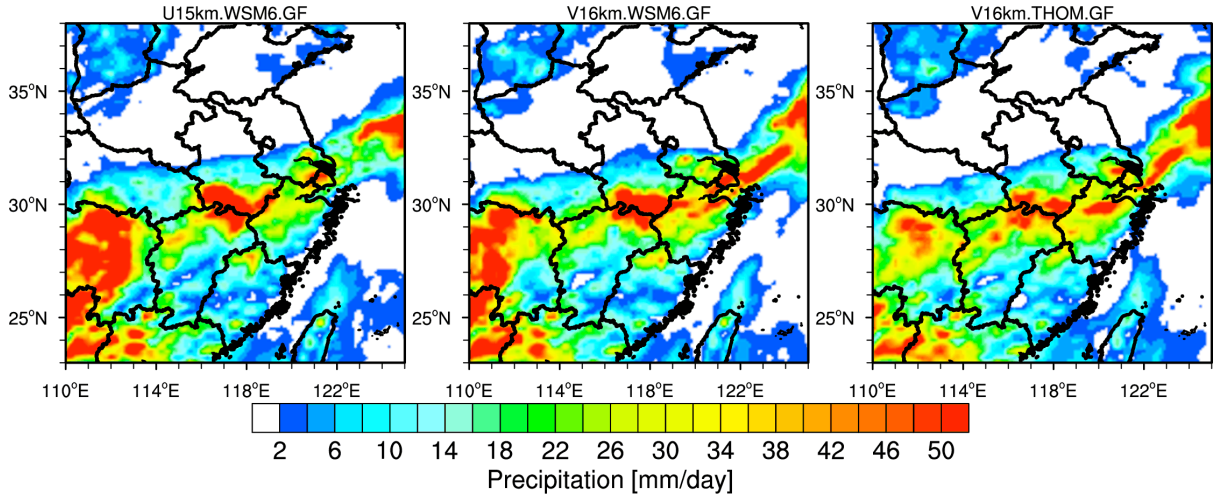


Figure S1 Zonal distributions of precipitation averaged during the event (June 25 00:00 to June 27 12:00 UTC time) over East China (denoted as the black box in Fig. 2) from the CMA station observations and the simulations with the global uniform (15 km, solid lines) and variable (16 km over the refined region as shown in Fig. 1c, dash lines) resolutions with two cloud microphysics parameterizations (WSM6, red dash lines; Thompson, green dash lines). The modeling results are sampled at the CMA station.



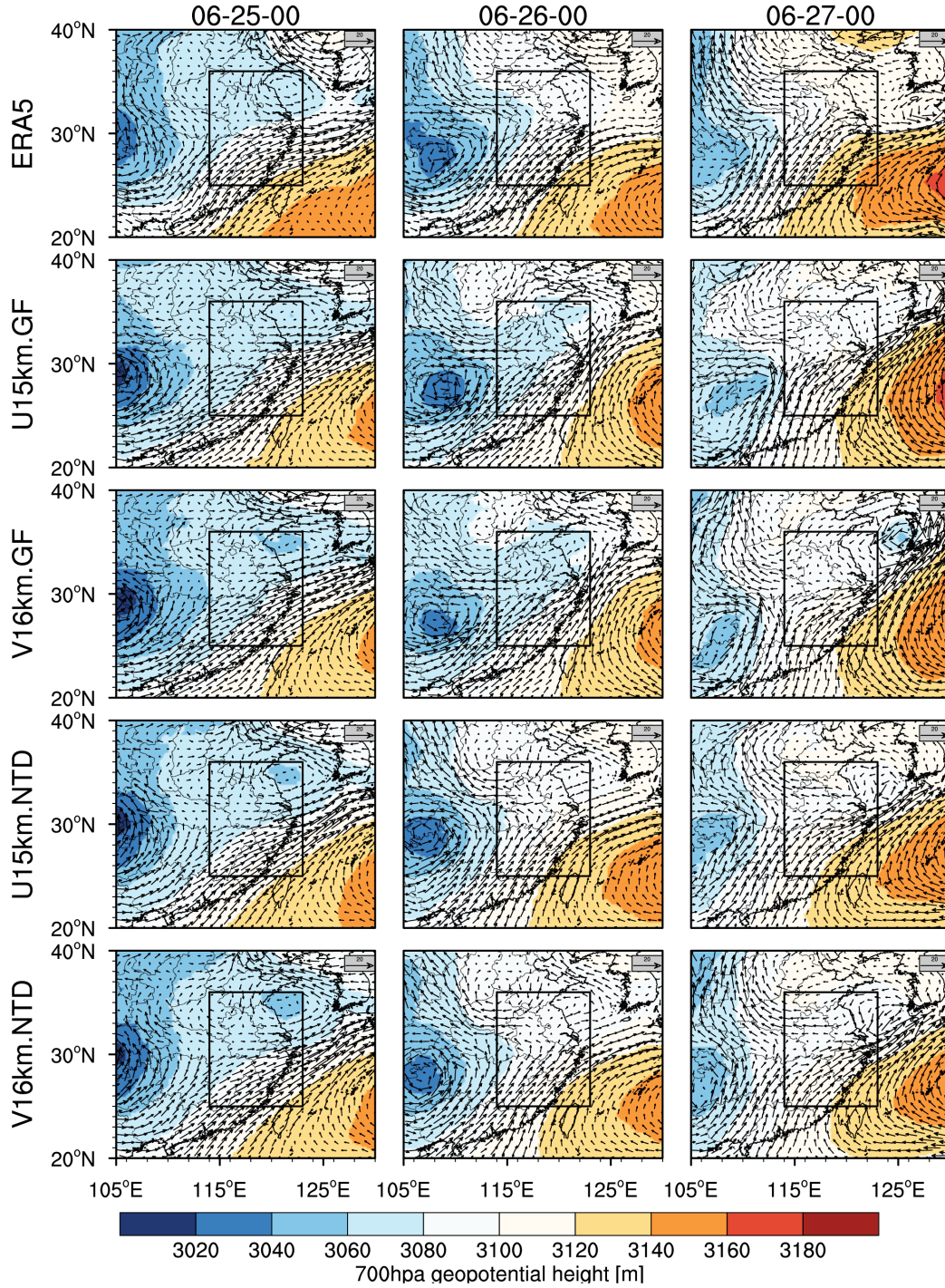


Figure S4 Spatial distributions of geopotential height and wind fields at 700 hPa at UTC 0000 of each day during the simulation (June 23 00:00 to June 27 00:00 UTC time) from the simulations with the global uniform (15 km) and variable (16 km over the refined region as shown in Fig. 1c) resolutions. The black box denotes the region for the analysis in this study.

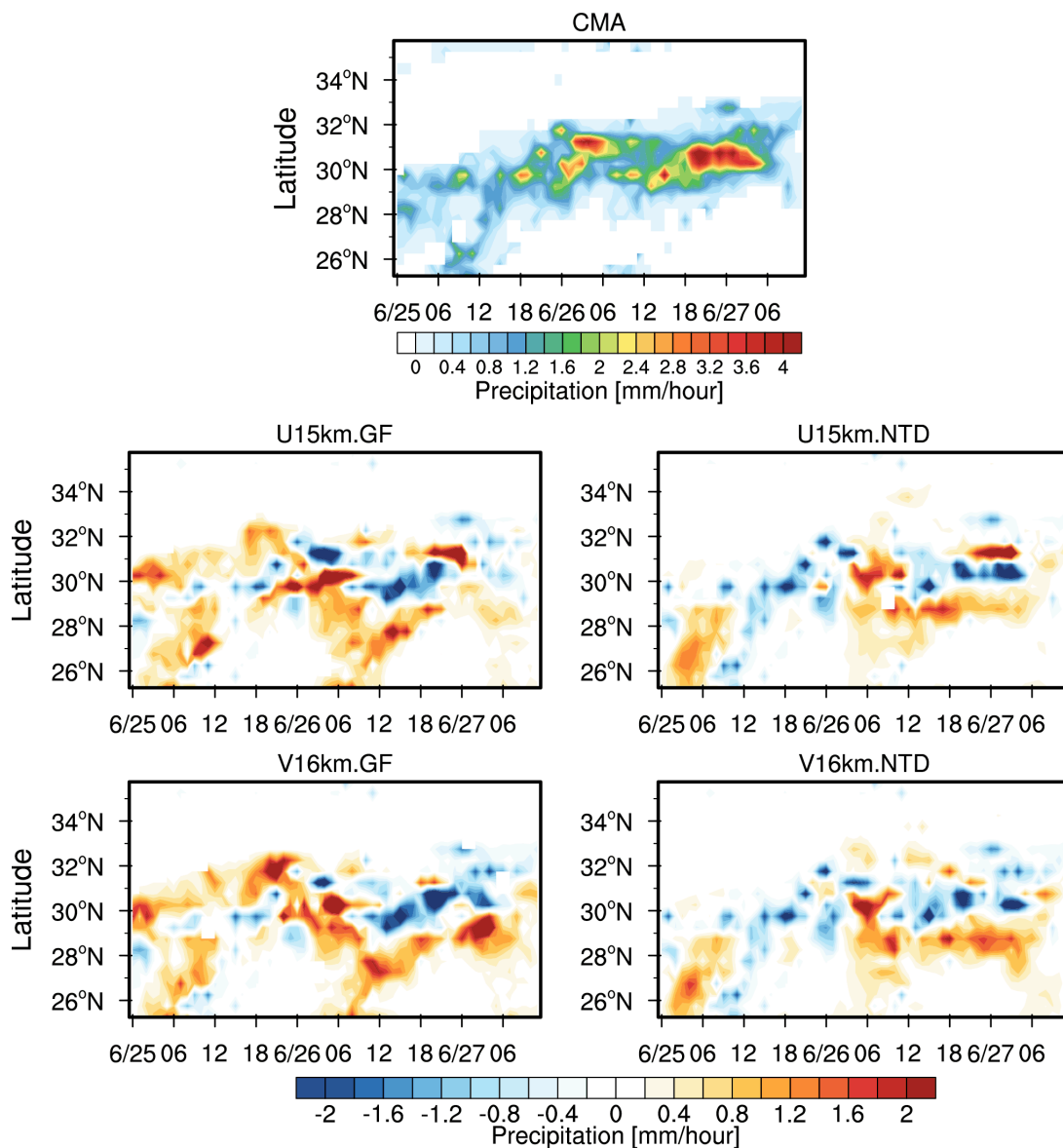


Figure S5 Time-Latitude cross section of precipitation during the event over East China from the CMA station observations and difference between the CMA and the simulations (simulation minus observation) with the global uniform and variable resolutions with two convective parameterizations. The modeling results are sampled at the CMA stations.

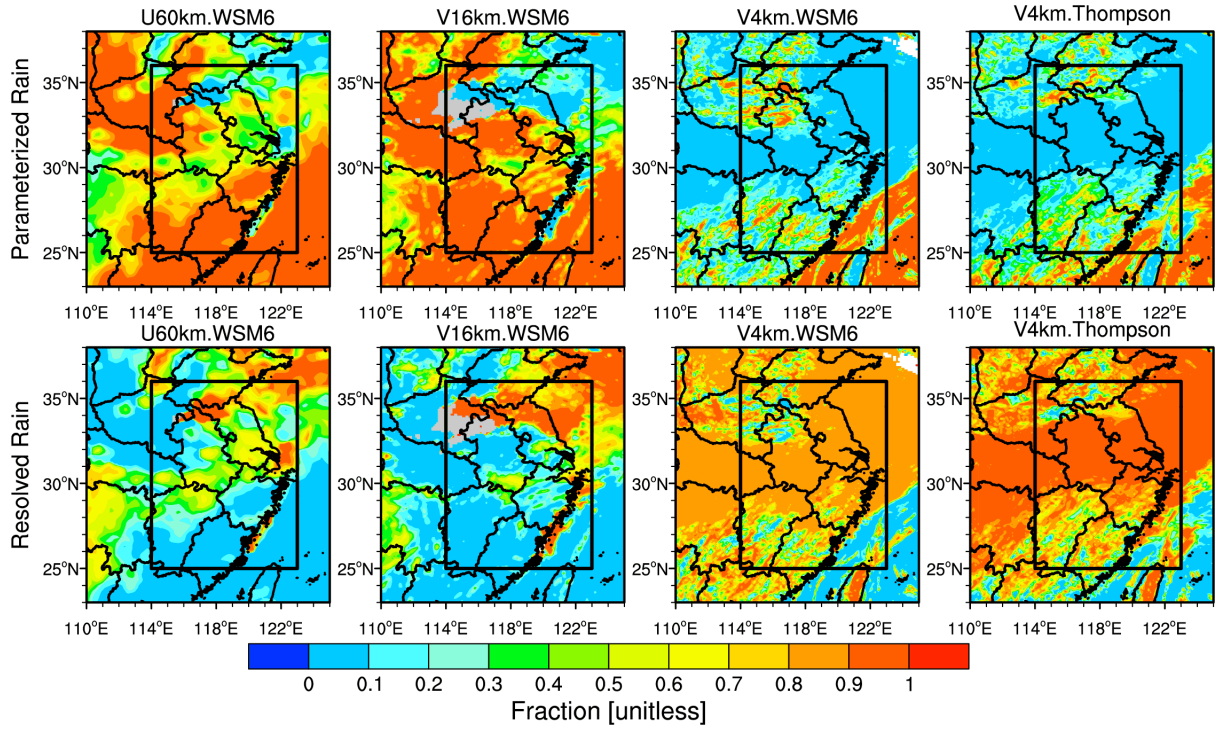


Figure S6 Spatial distribution of fraction of averaged parameterized and resolved precipitation in total precipitation during the event over East China from the simulations with the resolutions of 60 km, 16 km, and 4 km.

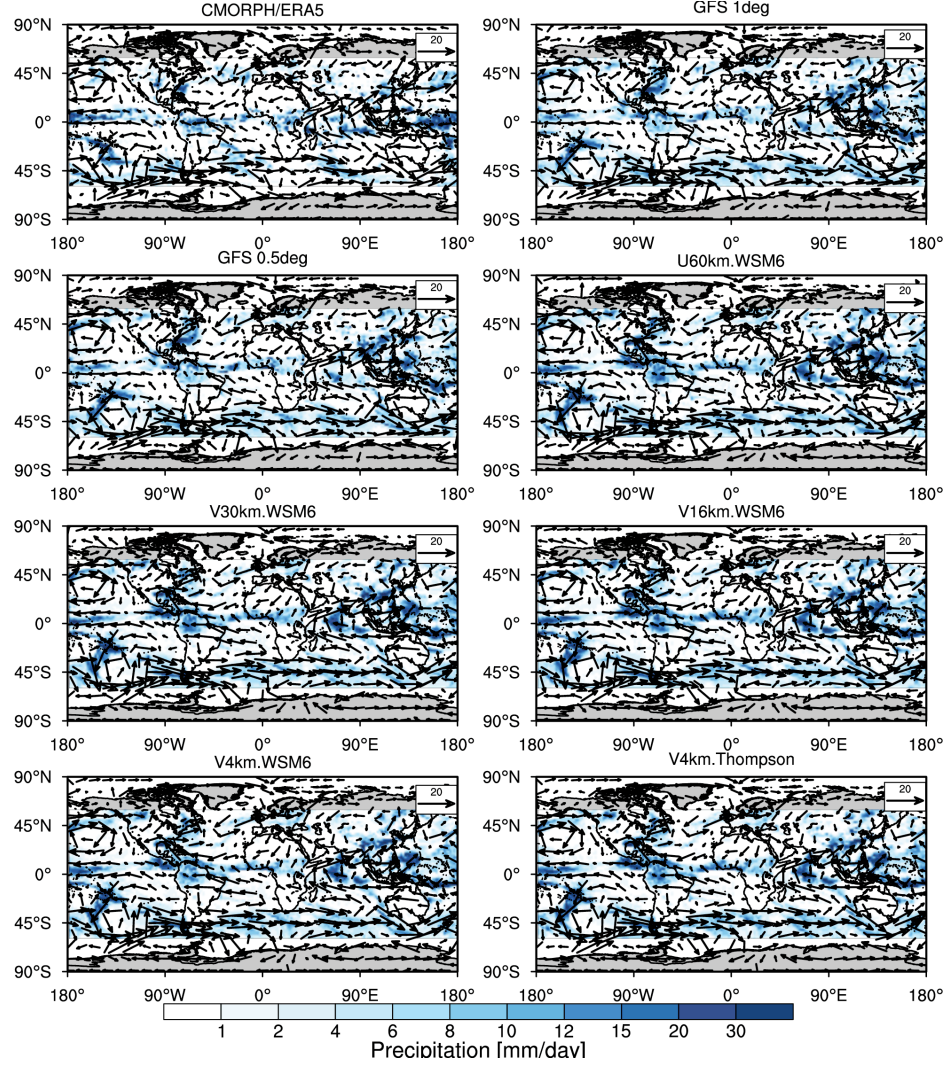


Figure S7 Global distributions of precipitation and wind fields at 850 hPa averaged during the event from the MPAS simulations at the resolutions of U60 km, V30 km, V16 km, and V4 km. The observed mean precipitation from the CMORPH satellite retrievals (downloaded from <https://climatedataguide.ucar.edu/climate-data/cmorph-cpc-morphing-technique-high-resolution-precipitation-60s-60n>) and the wind fields from the ERA5 reanalysis are shown as well. The black box denotes the region for the analysis in the following. For comparison, the GFS forecasts at 1 degree and 0.5 degree resolutions are also shown.

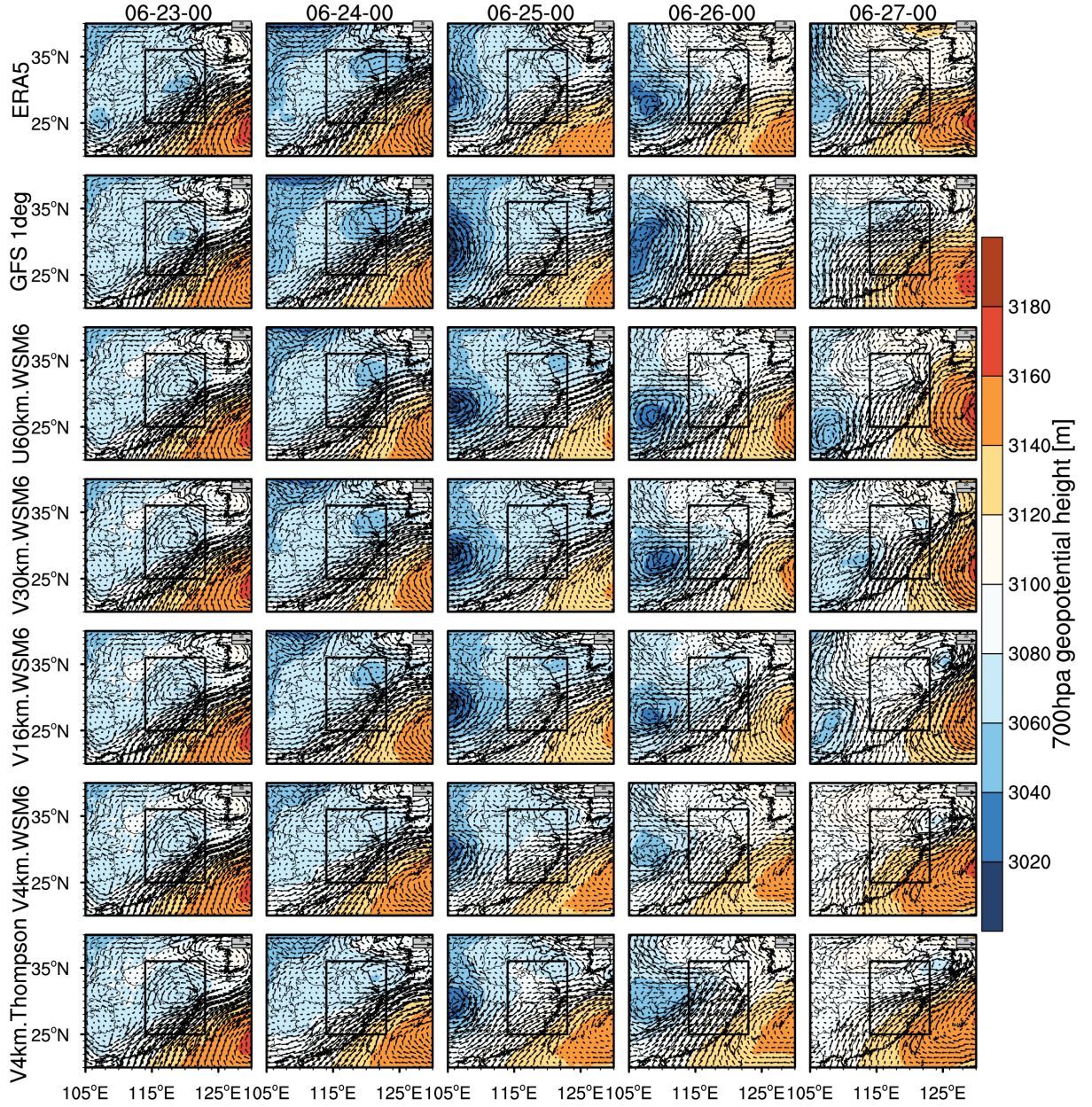


Figure S8 Spatial distributions of geopotential height and wind fields at 700 hPa at UTC 0000 of each day during the simulation (June 23 00:00 to June 27 00:00 UTC time) from the MPAS simulations at the resolutions of 60 km, 30 km, 16 km, and 4 km. The black box denotes the region for the analysis in this study. For comparison, the GFS forecast at 1 degree resolution is also shown.

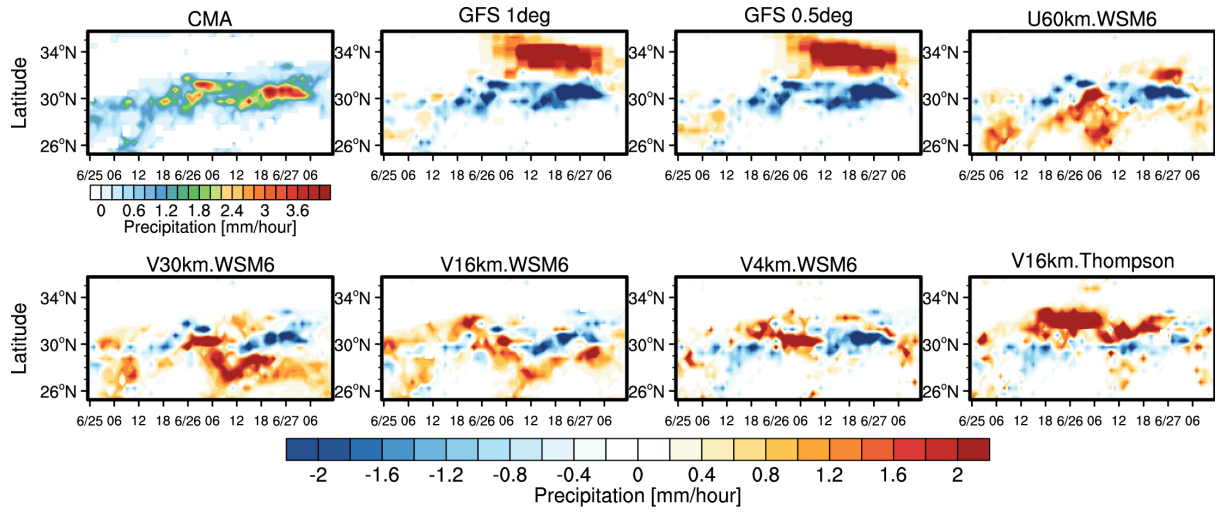


Figure S9 Time-Latitude cross section of precipitation during the event over East China from the CMA station observations and difference between the CMA and the simulations (simulation minus observation) with the global uniform and variable resolutions with two convective parameterizations. The modeling results are sampled at the CMA stations.

Modeling extreme precipitation over East China with a global variable-resolution modeling framework (MPASv5.2): Impacts of resolution and physics

¹Chun Zhao, ¹Mingyue Xu, ¹Yu Wang*, ¹Meixin Zhang, ²Jianping Guo, ³Zhiyuan Hu, ⁴L. Ruby Leung, ⁵Michael Duda, ⁵William Skamarock

¹School of Earth and Space Sciences, University of Science and Technology of China, Hefei, China

²State Key Laboratory of Severe Weather, Chinese Academy of Meteorological Sciences, Beijing, China

³Key Laboratory for Semi-Arid Climate Change of the Ministry of Education, Lanzhou University, Gansu, China

⁴Atmospheric Sciences and Global Change Division, Pacific Northwest National Laboratory, Richland, WA, USA

⁵National Center for Atmospheric Research, Boulder, CO, USA

Manuscript for submission to Geoscientific Model Development

*Corresponding authors: Yu Wang (wangyu09@ustc.edu.cn)

Key points:

1. MPAS simulations at global uniform and variable resolutions share similar characteristics of precipitation and wind in the refined region.
2. Numerical experiments reveal significant impacts of resolution on simulating the distribution and intensity of precipitation and updrafts.
3. Study provides evidence supporting the use of convection-permitting global variable-resolution simulation for studying extreme precipitation.

Deleted: The

Deleted: the

Deleted: the

Deleted: using

36 Abstract

37 The non-hydrostatic atmospheric Model for Prediction Across Scales (MPAS-A), a
38 global variable-resolution modeling framework, is applied at a range of resolutions from
39 hydrostatic (60 km, 30 km, 16 km) to non-hydrostatic (4 km) scales using regional refinement
40 over East Asia to simulate an extreme precipitation event. The event is triggered by a typical
41 wind shear in the lower layer of the Meiyu front in East China during 25-27 June 2012 of the
42 East Asian summer monsoon season. The simulations are evaluated using ground observations
43 and reanalysis data. The simulated distribution and intensity of precipitation are analyzed to
44 investigate the sensitivity to model configuration, resolution, and physics parameterizations. In
45 general, simulations using global uniform-resolution and variable-resolution meshes share
46 similar characteristics of precipitation and wind in the refined region with comparable
47 horizontal resolution. Further experiments at multiple resolutions reveal the significant impacts
48 of horizontal resolution on simulating the distribution and intensity of precipitation and
49 updrafts. More specifically, simulations at coarser resolutions shift the zonal distribution of the
50 rain belt and produce weaker heavy-precipitation centers that are misplaced relative to the
51 observed locations. In comparison, simulations employing 4 km cell spacing produce more
52 realistic features of precipitation and wind. The difference among experiments in modeling
53 rain belt features is found mainly due to the difference of simulated wind shear formation and
54 evolution during this event. Sensitivity experiments show that cloud microphysics have
55 significant effects on modeling precipitation at non-hydrostatic scales, but their impacts are
56 relatively small compared to that of convective parameterizations for simulations at hydrostatic
57 scales. This study provides the first evidence supporting the use of convection-permitting
58 global variable-resolution simulations for studying and improving forecasting of extreme
59 precipitation over East China, and motivates the need for a more systematic study of heavy
60 precipitation events and impacts of physics parameterizations and topography in the future.

Deleted: over

Formatted: Font color: Text 1

Formatted: Font color: Text 1

Deleted: China

Deleted: rainbelt

Deleted: negligible

69 **1. Introduction**

70 Extreme precipitation receives great attention because of its potential for generating
71 flood, landslide, and other hazardous conditions. East China, occupied by more than 70% of
72 the total population of China, is one of the areas with the most frequent intense extreme
73 precipitation around the world (Zhai et al., 2005; Li et al., 2016). The socioeconomic
74 development in regions such as the Yangtze River Delta region (YRD) in East China is
75 remarkably vulnerable to extreme precipitation, making accurate forecast of extreme
76 precipitation of great importance. The spatiotemporal variations of extreme precipitation over
77 East China and their possible causes and underlying mechanisms have been investigated in
78 many previous studies using observations and models (e.g., Ding et al., 2008; Zhang H. et al.,
79 2011; Li et al., 2013; Zhang Q. et al., 2015, 2017; Hui et al., 2015; Liu et al., 2015; Li et al.,
80 2016; Lin and Wang, 2016; Zhao et al., 2016; Zheng et al., 2016). Zhang et al. (2017)
81 established a relationship between the western North Pacific subtropical high (WNPSH) and
82 precipitation over East China and explored the underlying processes. Liu et al. (2015) analyzed
83 data from the meteorological stations in East China and found significant increases in heavy
84 precipitation at both rural and urban stations during 1955-2011. This enhanced precipitation
85 intensity in East China has been partly attributed to localized daytime precipitation events (Guo
86 et al., 2017). Recently, a regional climate model was used to simulate the regional climate
87 extremes of China and noted large sensitivity of the simulated summer heavy precipitation over
88 East China to the choice of cumulus parameterizations (Hui et al., 2015).

89 Numerical modeling is an important tool for understanding the underlying mechanisms
90 of extreme precipitation and predicting precipitation characteristics that contributes to
91 environmental impacts. Although precipitation modeling has improved in the last decades,
92 accurate prediction of extreme precipitation remains challenging because of the multiscale
93 nonlinear interactions of processes that generate heavy rainfall (Fritsch et al., 2004; Zhang et
94 al., 2011; Sukovich et al. 2014). Although not a panacea for weather and climate modeling
95 (NRC, 2012), previous studies suggested that increasing grid resolution could significantly
96 improve modeling of extreme precipitation because the impacts of topography, land-use, land-
97 atmosphere interaction, and other important processes are better resolved (e.g., Giorgi and
98 Mearns, 1991; Giorgi and Marinucci, 1996; Leung et al., 2003; Bacmeister et al. 2014;
99 ECMWF2016). With advances in computing and numerical modeling, convection-permitting
100 modeling offers even more hope for reducing biases in simulating precipitation as convection
101 and the strong vertical motions that are key to generating extreme precipitation are more

Deleted: Previous

103 explicitly resolved (Pedersen and Winther, 2005; Déqué et al., 2007; Gao et al., 2017; Yang et
104 al. 2017; Prein et al., 2015, 2017). Previous studies suggested that convection-permitting
105 modeling is needed for more accurate prediction of the timing, distribution, and intensity of
106 extreme precipitation events over China (e.g., Zhang et al., 2013; Xu et al., 2015).

107 Most studies of convection-permitting simulations have adopted non-hydrostatic
108 regional models developed for weather forecasting or regional climate modeling (Prein et al.
109 2015). Global models capable of simulating non-hydrostatic dynamics are not as common as
110 regional models, but they offer some advantages including the ability to provide global
111 forecasts or simulations while avoiding numerical issues associated with lateral boundary
112 conditions that are major sources of uncertainty in regional modeling and also limit regional
113 feedback to large-scale circulation (e.g., Giorgi and Mearns, 1999; Wang et al. 2004; Laprise
114 et al., 2008; Leung 2013; Prein et al. 2015). Non-hydrostatic global-variable resolution models,
115 in particular, are useful as they allow convection-permitting simulations to be performed using
116 regional refinement that significantly reduces computational cost compared to global
117 convection-permitting modeling. Although global hydrostatic variable-resolution climate
118 models, such as the variable-resolution version of Community Earth System Model, have been
119 used in various applications in the last few years (e.g., Rauscher et al., 2013; Zarzycki et al.,
120 2014, 2015; Rhoades et al., 2016; Huang et al., 2016; Wu et al., 2017; Gettelman, et al., 2018;
121 Wang et al., 2018; Burakowski et al., 2019), so far, few studies used global non-hydrostatic
122 variable-resolution models to investigate weather or climate simulations, particularly at
123 convection-permitting scales (e.g., Prein et al., 2015). This study explores the use of a non-
124 hydrostatic global variable resolution model, the Model for Prediction Across Scales (MPAS)
125 for modeling an extreme precipitation event in East China.

126 MPAS is a new multiscale modeling approach developed to take advantage of advances
127 in mesh generation by employing the spherical centroidal Voronoi tessellations (SCVTs) (Du
128 et al. 1999; Ringler et al. 2008). The SCVTs in MPAS enable local mesh refinement through
129 the mesh generation process where a specified scalar density function determines higher and
130 lower resolution regions in the mesh (see, e.g., Ju et al. 2011). Meshes can be configured with
131 multiple high-resolution regions, and high resolution in one region does not need to be balanced
132 by coarser resolution elsewhere. The underlying theory of SCVTs is robust concerning mesh
133 properties and mesh generation. The atmospheric solver in MPAS (Skamarock et al, 2012)
134 integrates the non-hydrostatic equations, and as such it is suitable for both weather and climate
135 simulation, i.e. for both nonhydrostatic and hydrostatic flow simulation. MPAS has been
136 evaluated and used in previous studies for investigating the resolution impact on modeling

Deleted: global

Deleted: 2012

Deleted: So

Deleted: ,

Formatted: English (US)

clouds and precipitation (O'Brien et al., 2013; Zhao et al., 2016), the structure of the inter-tropical convergence zone (ITCZ) (Landu et al., 2014), precipitation extremes (Yang et al., 2014), atmospheric river frequency (Hagos et al., 2015), the position and strength of the eddy-driven jet (Lu et al., 2015), global atmospheric predictability at convection-permitting scales (Judt, 2018), and regional climate modeling (Sakaguchi et al., 2015, 2016). Except for Zhao et al. (2016) and Judt (2018), the aforementioned studies used a hydrostatic version of MPAS applied at resolutions ranging from ~25 km to 200 km.

Deleted: Falko

To date, few studies have examined the MPAS performance in modeling extreme precipitation event, particularly at grid scales of ~10 km or less. In this study, we examine the MPAS performance in simulating a heavy precipitation event over East China and investigate its sensitivity to horizontal resolution and physics parameterizations. A heavy precipitation event that occurred on June 25-27 of 2012 over the YRD of East China is selected, as it is one of the ten heaviest precipitation events in 2012. This rainfall event was triggered by a typical southwest vortex in the middle and high troposphere and wind shear in the lower layer of Meiyu front over East China during the East Asian summer monsoon (e.g., Xiang et al., 2013; Yao et al., 2017), initiated around 1200 UTC of 25 June. Most (more than two third) of heavy precipitation events over East China were caused by the wind shear of Meiyu front in last decades (Yao et al., 2017). During this period, a heavy precipitating system propagated along the Yangtze River and produced as much as 244 mm of precipitation in 24 hours at some locations. The continuous precipitation led to 17 deaths and about RMB 3.68 billion in total damage, and affected more than 685 million people in the provinces of Central and East China.

Deleted: .

Formatted: Font color: Text 1

Formatted: Font color: Text 1

Simulations are performed using MPAS (v5.2) with different cumulus and microphysics schemes. We first compare simulations produced using a global mesh with uniform resolution and a global variable resolution mesh with a refined region that has the same resolution as that of the global uniform mesh. The goal is to demonstrate the fidelity of global variable resolution modeling relative to the more computationally expensive global high-resolution modeling approach in regions that share the same horizontal resolution. The impacts of resolutions at hydrostatic scales (with convective parameterizations) and non-hydrostatic scales (i.e., convection-permitting scales with convection processes largely resolved) are also examined. The MPAS simulations are evaluated against weather station observations from the National Meteorological Information Center of the China Meteorological Administration (CMA). In addition, the modeling results are also compared with the forecasts produced by the Global Forecast System (GFS) of the National Centers for Environmental Prediction (NCEP).

The rest of the paper is organized as follows. Section 2 describes briefly the MPAS model, the physics parameterizations, and the model configuration for this study, followed by a description of data for evaluation. The series of global uniform and variable resolution experiments are analyzed in section 3. The findings are then summarized in section 4.

2. Data and methodology

2.1 Model and experiments

2.1.1 MPAS-Atmosphere (MPAS-A) model

This study uses a fully compressible non-hydrostatic model (MPAS v5.2) developed for weather prediction and climate applications. The non-hydrostatic dynamical core of MPAS is described in Skamarock et al. (2012). MPAS uses C-grid staggering of the prognostic variables and centroidal Voronoi meshes to discretize the sphere. The unstructured spherical centroidal Voronoi tessellation (SCVT) generation algorithms can provide global quasi-uniform resolution meshes as well as variable-resolution meshes through the use of a single scalar density function, hence opening opportunities for regional downscaling and upscaling between mesoscales and non-hydrostatic scales to hydrostatic scales within a global framework. The vertical discretization uses the height-based hybrid terrain-following coordinate (Klemp, 2011), in which coordinate surfaces are progressively smoothed with height to remove the impact of small-scale terrain structures. The dynamical solver applies the split-explicit technique (Klemp et al., 2007) to integrate the flux-form compressible equations. The basic temporal discretization uses the third order Runge-Kutta scheme and explicit time-splitting technique (Wicker and Skamarock, 2002), similar to that used in the Weather Research and Forecasting (WRF) model (Skamarock et al., 2008). The scalar transport scheme used by MPAS on its Voronoi mesh is described in Skamarock and Gassmann (2011), and the monotonic option is used for all moist species. The extensive tests of MPAS using idealized and realistic cases verify that smooth transitions between the fine- and coarse-resolution regions of the mesh lead to no significant distortions of the atmospheric flow (e.g., Skamarock et al., 2012; Park et al., 2013).

In the current version (v5.2) of MPAS, there are a few physics schemes available. Three convective parameterizations can be used. The Kain-Fritsch (KF, Kain, 2004) and the new Tiedtke (NTD, Bechtold et al., 2004, 2008, 2014) schemes represent both deep and shallow convection using a mass flux approach with a convective available potential energy (CAPE) removal time scale (Kain, 2004). The third one, the GF scheme (Grell and Freitas, 2014), is

based on the Grell-Devenyi ensemble scheme (Grell and Devenyi, 2002) using the multi-closure, multi-parameter, ensemble method but with improvements to smooth the transition to cloud-resolving scales following Arakawa et al. (2011). This scale-awareness is critical for global variable resolution simulation across hydrostatic (e.g., tens of km) and non-hydrostatic scales (e.g., 4 km). Fowler et al. (2016) implemented the GF convective parameterization in MPAS and examined the impacts of horizontal resolution on the partitioning between convective-parameterized and grid-resolved precipitation using a variable-resolution mesh in which the horizontal resolution varies between hydrostatic scales (~50 km) in the coarsest region of the mesh to non-hydrostatic scales (~3 km) in the most refined region of the mesh. For cloud microphysics, the WSM6 (Hong and Lim, 2006) and Thompson (Thompson et al., 2008) schemes, both of which are bulk microphysical parameterizations, are selected and compared. Both schemes include six hydrometeor species: water vapor, cloud water, rain, cloud ice, snow, and graupel (Gettelman et al., 2019). The WSM6 scheme is a one-moment prognostic parameterization, while the Thompson scheme includes a two-moment prognostic parameterization for cloud ice and the single-moment parameterization for the other hydrometeor species. The two schemes apply the same formula of gamma distribution of hydrometeor species: $N(D) = N_0 D^\mu e^{-\lambda D}$, where D is the particle diameter, N_0 is the intercept parameter, μ is the shape factor, and λ is the slope parameter, although the parameter values or functions vary in the two schemes. The mass-size relationship in WSM6 and Thompson is also expressed in the same formula as $m(D) = aD^b$. The mean falling speed is calculated as $V(D) = cD^d (\frac{\rho_0}{\rho})^{0.5}$ in WSM6 and $V(D) = cD^d (\frac{\rho_0}{\rho})^{0.5} \exp(-fD)$ in Thompson, respectively (Hong and Lim, 2006; Thompson et al., 2008). In the formula, the WSM6 scheme assumes a power-law fit between terminal velocity and particle size as Locatelli and Hobbs (1974), while the Thompson scheme incorporates an exponential decay parameter to allow for a decrease in falling speed with increasing size (Molthan et al., 2012). Two options are available for representing the planetary boundary layer processes, the Mellor-Yamada-Nakanishi-Niino (MYNN) scheme (Nakanishi and Niino, 2006 and 2009) and the YSU scheme (Hong et al., 2006; Hong 2010). The Noah scheme (Chen and Dudhia, 2001) and the RRTMG scheme (Mlawer et al., 1997; Iacono et al., 2000) were implemented, respectively, for the land surface and radiative transfer processes.

Deleted: are selected.

2.1.2 Numerical experiments

242 In this study, the height coordinate of MPAS is configured with 55 layers, and the model
243 top is at 30 km. Multiple experiments are conducted with MPAS using quasi-uniform
244 resolution meshes and variable resolution meshes. Two quasi-uniform resolution meshes and
245 three variable resolution meshes are configured, similar to those shown in Figure 1a and b that
246 are coarsened to display the structure of the individual mesh cells. The quasi-uniform mesh has
247 essentially the same mesh spacing globally, while the variable resolution mesh has finer mesh
248 spacing in the refined region with a transition zone between the fine and coarse resolution
249 meshes. More details about the mesh generation can be found in Ringler et al. (2011). The two
250 quasi-uniform meshes have grid spacing that approximately equals to 15 km (U15km) and 60
251 km (U60km). The three variable resolution meshes feature a circular refined high-resolution
252 region centered over East China as shown in Figure 1c. Figure 1c shows the exact mesh size
253 distribution of the 4-60km variable resolution mesh (V4km) that has a refined region with grid
254 spacing of approximately 4 km, and the mesh spacing gradually increases through a transition
255 zone to approximately 60 km for the rest of the globe. The other two variable resolution meshes
256 (V16km and V30km) have a similar mesh structure as the V4km mesh but with a mesh spacing
257 of 16 km and 30 km, respectively, over the refined region that gradually increases to 128 km
258 and 120 km, respectively, elsewhere.

259 Experiments U15km and V16km are compared to examine the difference between
260 global uniform and variable resolution simulations in capturing the precipitation in the refined
261 region, in order to explore the potential of regional refinement for regional weather and climate
262 simulation. It is noteworthy here that the U15km mesh comprises ~2.5 million cells and the
263 V16km mesh only comprises ~0.11 million cells. The difference in the number of mesh cells
264 leads to a difference in computational and storage demand. With the TH-2 supercomputer of
265 National Supercomputer Center in Guangzhou (NSCC-GZ), it takes ~9000 CPU hours and
266 ~240 CPU hours to finish a one-day simulation for U15km and V16km, respectively. In
267 addition, with the standard MPASv5.2, the sizes of output data per one-day simulation for
268 U15km and V16km are 0.5 T and 0.02 T, respectively. The same time step of 60 second is used
269 for physics and dynamics for both U15km and V16km simulations. In order to investigate the
270 potential impact from physics parameterizations, two available convective parameterizations
271 (GF and NTD) are used for each experiment with the two meshes. Two cloud microphysics
272 schemes (WSM6 and Thompson) are also tested, but the precipitation differences in the U15km
273 and V16km experiments are small. Therefore, only the results using WSM6 with two different
274 convective parameterizations are shown in this study for the two meshes (U15km.NTD,
275 U15km.GF, V16km.NTD, and V16km.GF).

276 The U60km, V30km, V16km, and V4km experiments are conducted to quantify the impacts
277 of horizontal resolution on simulating precipitation characteristics. The numbers of grid cells
278 in the U60km, V30km, V16km, and V4km meshes are ~0.16 million, 0.10 million, ~0.11
279 million, and ~0.8 million, respectively. Difference in the number of cell and minimum cell size
280 also leads to a difference in computational and storage demand. With the TH-2 supercomputer
281 of NSCC-GZ, it takes ~200 CPU hours, ~150 CPU hours, ~240 CPU hours, and ~1800 CPU
282 hours to finish a one-day simulation for U60km, V30km, V16km, and V4km meshes,
283 respectively. In addition, with the standard MPASv5.2, the sizes of output data per one-day
284 simulation for the four meshes are 0.03 T, 0.02 T, 0.02 T, and 0.15 T, respectively. The time
285 steps used for physics and dynamics for the four meshes are 300 seconds, 120 seconds, 60
286 seconds, and 20 seconds, respectively.

287 As discussed above, GF is the only convective parameterization that has been tested
288 with scale-aware capability for using across the hydrostatic (e.g., tens of km) and non-
289 hydrostatic scales (e.g., 4 km). Therefore, in order to investigate the difference among the
290 experiments with the four meshes (U60km, V30km, V16km, and V4km), they are all
291 conducted with the GF convective parameterization. Since the cloud microphysics has
292 significant impact on the V4km simulations (discussed latter), the experiments of V4km with
293 both WSM6 (V4km.WSM6) and Thompson (V4km.Thompson) cloud microphysics schemes
294 are analyzed in this study. When examining the difference between the global uniform and
295 variable resolution simulations and investigating the impact of mesh spacing, the same physics
296 schemes and parameter values are used in multiple experiments if not specified explicitly. All
297 the numerical experiments discussed above are summarized in Table 1.

298 Due to the large computing cost and data storage of the experiments conducted,
299 particularly for the U15km and V4km experiments, this study does not perform ensemble
300 simulations. Instead, the bootstrapping statistical analysis is used to test the statistical
301 significance of the difference among multiple experiments investigated in this study. The
302 bootstrap method uses resampling technique to extract certain samples, called bootstrap
303 samples, within the range of the original data. Statistical metrics, such as averages, variances,
304 correlation coefficient, can be calculated for each bootstrap sample. For a given confidence
305 level (e.g., 95%), bootstrap confidence intervals of specific statistical metric can be estimated
306 (e.g., Efron, 1992; Efron and Tibshirani, 1994).

307 To simulate the heavy precipitation event that occurred during June 25-27 of 2012 over
308 the YRD of East China, all the MPAS experiments were initialized at 0000 UTC of 23 June
309 2012 to allow appropriate spin-up time, and the modeling results for 25-27 June 2012 are

Deleted: and can be used

Deleted: .

Formatted: Indent: First line: 1.27 cm

analyzed. The simulations were initialized using the [analysis data](#) at 1° horizontal resolution at 0000 UTC of 23 June 2012 from the Global Forecast System (GFS) of National Center for Environmental Prediction (NCEP), [the same as that used by the GFS forecast for the period.](#) This way, the MPAS simulation results can also be compared against the GFS forecast starting from the 0000 UTC of 23 June 2012.

2.2 Dataset

Several datasets are used to evaluate the MPAS simulations. The hourly precipitation dataset from CMA is used for evaluating the simulated precipitation characteristics. The distribution of stations over the study domain is shown as the color-filled circles in Figure 2. The hourly wind field dataset from the ECMWF Reanalysis ([ERA5](#)) ([0.28°×0.28°](#)) (<https://rda.ucar.edu/datasets/ds630.0/>) is used as the reference for evaluating the simulated distributions of winds. Lastly, the global forecast products at 0.5° and 1° horizontal resolutions starting from UTC00 of 23 June 2012 are also used for comparison. The GFS forecast products are downloaded from <https://www.ncdc.noaa.gov/data-access/model-data/model-datasets/global-forecast-system-gfs>. Since the focus of this study is not to investigate the difference between MPAS and GFS [or to evaluate the performance of GFS](#), details about the GFS are not discussed here but can be found on the website listed above.

329

3. Results

3.1 Simulations at quasi-uniform and variable resolutions

Figure 2 shows the spatial distributions of precipitation and wind at 850 hPa averaged during the event (June 25 00:00 to June 27 12:00 UTC Time) from the simulations with global uniform (15 km) and variable (16 km over East China) resolutions (U15km.NTD and V16km.NTD). The mean precipitation from the CMA stations and the winds from the ERA-interim reanalysis are also shown. The CMA observations show average precipitation rate exceeding 50 mm/day over central East China with a heavy rain belt extending from west to east [along 31°N](#). The rain belt is [associated with the wind shear near the surface that is typically accompanied with](#) the Meiyu front [during the East Asian summer monsoon](#). In general, both simulations capture the observed precipitation pattern. It is evident that the modeling results over the refined region are consistent between the uniform and variable [resolution simulations](#). The spatial correlation coefficient between the two simulations over the refined region ([entire region shown in](#) Fig. 2) is 0.85. Besides precipitation, both simulations also capture the

Deleted: forecast

Deleted:).

Deleted: 6-

Deleted: interim

Deleted: ERA-interim

Deleted: 75° ×

Deleted: 75°) (Dee et al., 2011)

Deleted: part of

Deleted: that generates a large fraction of precipitation

Deleted: in China

Deleted: resolutions.

distribution of winds from the reanalysis data. The wind fields between the two simulations are also consistent with a [spatial](#) correlation coefficient of 0.99.

As mentioned above, the precipitation during this event is concentrated in a west-east narrow belt. For a more quantitative comparison, Figure 3 shows the zonal averaged precipitation during the event over East China (denoted as the black box in Fig. 2) from observations and simulations. The CMA observations show an evident precipitation peak reaching ~40 mm/day around the latitude of 31°N. All four simulations with different resolutions and convective parameterizations capture well the zonal distribution of observed precipitation. The correlation coefficients are 0.9 and 0.89 for the U15km and V16km simulations with the GF scheme, respectively, and 0.89 and 0.86 for the same simulations but with the NTD scheme. This comparison further indicates that the simulations at global uniform and variable resolutions are consistent with each other, with only negligible impacts from different convective parameterizations. Although this consistency does not depend on the convective schemes, simulations with the GF parameterization produce larger peak precipitation than those with the NTD parameterization and are more consistent with observations for this event. The impact of [cloud](#) microphysics (WSM6 and Thompson) on [the consistency in modeling total precipitation](#) is also examined and is found to be negligible ([Fig. S1 and S2 in the supporting materials](#)), although there are some impacts on the simulated grid-resolved precipitation ([Fig. S3 in the supporting material](#)).

Figure 4 shows the meridional precipitation propagation over East China during the event. The CMA observations indicate that the rain belt propagates from 26°N at 06 UTC of 25 June to 31°N at 00 UTC of 26 June, [and includes two precipitation peaks around 31°N. The rainfall](#) reaches the first peak around 00 UTC of 26 June. The rain belt stays around 31°N and reaches the second peak around 00 UTC of 27 June. The event ends around 12 UTC of 27 June. [The first precipitation peak was generated by the southwest-northeast wind shear line formed over Central East China along with a vortex over the Southwest at 00 UTC of 26 June. The shear line gradually extended eastward, leading to the second precipitation peak around 00 UTC of 27 June \(Fig. S4 in the supporting material\). All four experiments generally simulate the southwest vortex and wind shear during the event, although the strength and location do not match perfectly with the reanalysis. As the large-scale environment is quite well represented in the model, the simulations also generally capture the two peaks of precipitation along 31°N as observed. However, both U15km and V16km simulate a broader rain belt, resulting in positive biases of precipitation south of 30°N \(Fig. S5 in the supporting materials\).](#)

Deleted: not shown

Deleted: . The

Deleted: All four simulations generally reproduce the observed precipitation propagation.

Both simulations shift the first peak precipitation southward. In addition, the simulations extend the first peak precipitation period and shorten the second one to some extent (Fig. S5 in the supporting materials). The lower averaged total precipitation around 31°N from the simulation with the NTD parameterization (Fig. 3) is mainly due to the lower rainfall before 26 June compared to the one with the GF parameterization (Fig. S5). For the two precipitation peaks, the simulation with NTD is comparable to the one with GF. Although the two convective parameterizations lead to significant difference in simulating total precipitation before 26 June, both simulations generate consistent wind circulations at 700 hPa before 26 June with spatial correlation coefficients above 0.9 (over the domain as shown in Fig. S4 in the supporting material). Although the two convective parameterizations lead to different total precipitation, they have negligible impact on the consistency in modeling precipitation propagation using uniform and variable resolutions during this event. The correlation coefficients are 0.48 and 0.42 for the simulations with the GF scheme at the resolutions of U15km and V16km, respectively, and 0.55 and 0.54 for the simulations with the NTD scheme at the two resolutions. The results again indicate the consistency between the simulations at the global uniform and variable resolutions at hydrostatic scale over the refined region, regardless of the convective parameterization used.

Overall, for the selected event, the MPAS simulations at global uniform and variable resolutions produce consistent results over the refined region with comparable horizontal resolution in terms of the spatial patterns of precipitation and wind fields and the precipitation propagation. This finding is in general agreement with the findings by previous studies of MPAS with idealized experiments (e.g., Zhao et al., 2016) and real-world experiments (e.g., Sakaguchi et al., 2015). These findings provide the basis for using global variable resolution configurations of MPAS for modeling extreme precipitation over East China. In the following, the impacts of resolution on modeling extreme precipitation during this event are investigated with multiple global variable-resolution experiments.

3.2 Impacts of resolution

3.2.1 Parameterized and resolved precipitation

Multiple experiments using MPAS at various resolutions are conducted as stated in the methodology section. The resolution crosses the scales from 60 km, 30 km, 16 km to 4 km. For global variable resolution configurations, a scale-aware convective parameterization is needed, especially for the configuration that crosses the hydrostatic (convective parameterization is

Deleted: . The

Deleted: and microphysics (not shown) parameterizations have negligible impact on modeling precipitation propagation during this event.

required) and non-hydrostatic scales (convection-permitting). Therefore, the experiments analyzed below are all conducted with the GF scheme that is developed for simulations down to ~ 4 km resolution (details can be found in Grell and Freitas, 2014). To demonstrate the scale-aware performance of the GF convective parameterization across various resolutions, Figure 5 shows the spatial distributions of convective parameterized and resolved precipitation averaged during the event. At the resolution of 60 km and 16 km, precipitation produced from the convective parameterization dominates the total precipitation amount. On the contrary, at the resolution of 4 km, the total precipitation amount from simulations with two different microphysics is dominated by the resolved precipitation. The fraction of parameterized precipitation in the total decreases significantly from the simulations at 16 km to the ones at 4km over the heavy precipitation region (Fig. S6 in the supporting materials). It is also interesting that the fraction of parameterized precipitation increases from the simulations at 60 km to the ones at 16 km to some extent. This demonstrates that the GF scheme is aware of the resolution change so the precipitation from the simulations at convection-permitting scale is mostly produced by the cloud microphysics in MPAS.

3.2.2 Spatial and temporal variation

Figure 6 shows the observed and simulated spatial distributions of precipitation and wind fields at 850 hPa averaged during the event. For comparison, the GFS forecast results at the resolutions of 1.0 degree and 0.5 degree are also included. The GFS forecast results from the two resolutions are similar, both showing a northward shifted rain belt compared to the CMA observation. Due to the northern shift of the rain belt, the spatial correlation coefficients between the GFS and the CMA observations over the entire region of Fig. 6 are only 0.06 and 0.03 for the resolutions of 1.0 degree and 0.5 degree, respectively. In comparison, the spatial correlation coefficients between the CMA observations and the MPAS simulations at the resolutions of 60 km, 30 km, and 16 km are 0.49, 0.47, and 0.56, respectively. The correlation coefficients for the 4 km simulations with the WSM6 and Thompson microphysics schemes are 0.63 and 0.54, respectively. In general, the experiments at the convection-permitting scale (4 km) capture better the observed precipitation pattern than simulations with convective parameterization over the refined region, although the performance is affected by the microphysics scheme to some extent.

In order to test the statistical significance of the difference among the experiments, the 95% confidence intervals of spatial correlation are estimated based on the bootstrap analysis. Although the correlation coefficients estimated above have an uncertain range, at the 95% confidence level the results still indicate that the V16km simulation produces better spatial

463 pattern of precipitation than other hydrostatic-scale simulations. In addition, the simulation at
 464 the convection-permitting scale is comparable to, if not better than, the V16km simulation. The
 465 results are summarized in Table 2. It is noteworthy that, although the difference in precipitation
 466 over East China is significant among the GFS forecasts at 0.5° and 1.0° resolutions and MPAS
 467 at various resolutions, their global distributions of precipitation and wind averaged during the
 468 event period are similar with spatial correlation coefficients of 0.40-0.43 (precipitation) and
 469 0.86-0.93 (wind), respectively, against the satellite retrieved precipitation and ERA5 reanalysis
 470 wind (Fig. S7 in the supporting material).

471 The zonal distributions of precipitation can better demonstrate the difference among
 472 the simulations. Figure 7 shows the observed and simulated zonal distributions of precipitation
 473 averaged during the event over East China. For comparison, the GFS forecasts at 1° and 0.5°
 474 resolutions are also included. The modeling results are sampled at the CMA stations.
 475 Consistent with the spatial distributions of precipitation shown in Fig. 6, the GFS forecasts at
 476 both 0.5° and 1.0° resolutions reproduce the precipitation peak of ~40 mm/day but shift the
 477 rain belt northward by about 4.0° latitude from 31°N to 35°N. The MPAS simulations at 16
 478 km and 30 km with the GF scheme can well capture the peak precipitation around 31°N,
 479 although the simulation at 30 km produces a second lower peak of precipitation around 29°N.
 480 The simulation at 60 km produces much lower precipitation peak of ~25 mm/day and shifts the
 481 rain belt southward to around 30°N. The underestimate of the simulation at 60 km is mainly
 482 due to the underestimate of the convective parameterized rain (Fig. 5). For the two MPAS
 483 simulations at 4 km, the precipitation is mainly generated by cloud microphysics (Fig. 5) and
 484 therefore can be significantly affected by the cloud microphysics schemes. The MPAS
 485 simulations at 4 km with WSM6 and Thompson produce different zonal distributions of the
 486 rain belt. The simulation using WSM6 reproduces the peak of precipitation, while the
 487 simulation using Thompson produces higher precipitation with a peak at 50 mm/day and shifts
 488 the peak northward by about 1 degree. Overall, the correlation coefficients between the CMA
 489 observations and the GFS forecasts are -0.19 and -0.15 for 0.5° and 1.0°, respectively, and the
 490 correlation coefficients are 0.68, 0.71, 0.89, and 0.97 (0.72) for the MPAS simulations at 60
 491 km, 30 km, 16 km, and 4 km with the WSM6 (Thompson) cloud microphysics. At the 95%
 492 confidence level, the difference among the experiments is significant (Table 2).

493 Figure 8 compares the observed and simulated precipitation propagation during the
 494 event over East China. The modeling results are sampled at the CMA stations. The GFS
 495 forecasts at 0.5° and 1.0° are similar, and both generate a heavy precipitation zone between

Deleted: ,

Deleted: ECMWF

Deleted: not shown

Deleted: fairly well

34°N and 35°N that lasts for about 18 hours from UTC12 of June 26. This is largely different from the CMA observations, so the correlation coefficients between the forecasts and observations are only 0.02 and 0.03 for 0.5° and 1.0°, respectively. The northward shift of rain belt during the event (shown in Fig. 6 and 7) is related to the GFS forecast that only produced the second peak of precipitation around UTC 0000 of 27 June while totally missing the first peak. In addition, the GFS forecast overestimates the second peak and shift it towards the north by about 4°. The timing and location shift of the rain belt in the GFS forecast are mainly because of the bias of GFS in simulating the wind shear in this event. The GFS forecast failed to produce the southwest-northeast wind shear line around UTC 0000 of 26 June and generated too broad vortex over the west. Around UTC 0000 of 27 June, GFS simulated the wind shear line but locating it further north (Fig. S8 in the supporting material).

The MPAS simulations are highly dependent on the resolutions. All simulations roughly produce the two peaks of precipitation as observed during the event. However, the experiment at 60 km simulates the first precipitation peak southward and the second peak northward of the observations, while the experiment at 30 km simulates the second peak further south and a few hours earlier. The time and location shift corresponding well to biases in simulated wind shear (Fig. S8). The spatial correlation coefficients of precipitation are 0.30 and 0.32 between the observations and the simulations at 60 km and 30 km, respectively. The experiments at 16 km and 4 km with the WSM6 cloud microphysics scheme can better capture the timing and latitude of the observed precipitation event than U60km and V30km (Fig. S9 in the supporting materials), however both V16km and V4km overestimate the first peak precipitation and underestimate the second peak. The experiment at 4 km with the Thompson scheme overestimates the precipitation amount of both peaks. The correlation coefficients are 0.41 and 0.42 (0.38) for 16 km and 4 km with the WSM6 (Thompson) cloud microphysics schemes, respectively. At the 95% confidence level (Table 2), the experiments at 16 km and 4 km are comparable in terms of simulating the propagation of this rain belt and better than the experiments at other resolutions. It is interesting to note that MPAS and GFS forecasts, sharing the same initial condition, simulate different large-scale circulation particularly the wind shear structure with the system evolving (Fig. S8). The model capability in successfully capturing the wind shear structure during this event determines the performance in generating the rain belt evolution. The formation and evolution of wind shear during the Meiyu front over East China have been found interacting with multiscale processes and systems, including terrain and convective latent heat (Yao et al., 2017). Different representation of the terrain over East China

Formatted: Font color: Text 1

Deleted: reproduce

Deleted: at roughly the same time

Formatted: Font color: Text 1

Formatted: Font color: Text 1

Deleted: .

Formatted: Font color: Text 1

Formatted: Font color: Text 1

Formatted: Font color: Text 1

Formatted: Font color: Text 1

Deleted: well

Formatted: Font color: Text 1

Deleted: , except that the

Formatted: Font color: Text 1

Deleted: the first peak

Formatted: Font color: Text 1

Deleted: .

540 in various resolutions may impact the simulated wind shear structure. Previous studies also
541 found that convective latent heat may vary with resolutions and physics (Hagos et al., 2013;
542 Zhao et al., 2016), which can further affect the simulation of wind shear structure. Therefore,
543 the difference in resolution and physics between MPAS and GFS may result in their difference
544 in simulating the formation and evolution of wind shear structure during the event. A more
545 detailed exploration of the differences between the MPAS and GFS simulations is beyond the
546 scope of this study.

547 The spatial distribution of the rain belt can also be reflected by the vertical wind
548 distributions. Figure 9 compares the height-latitude cross section of the winds averaged over
549 the region (shown as in Fig. 6) during the event from the ERA5 reanalysis, the GFS forecasts,
550 and the MPAS simulations. In the ERA5 reanalysis wind fields, vertical motion is located
551 primarily around 31°N, extending from the lower troposphere (~900 hPa) to the upper
552 troposphere (~200 hPa). The GFS simulates the vertical motion primarily around 33°N, but the
553 vertical motion is also strong around 35°N from 600 hPa to 200 hPa, which can be linked to
554 the heavy precipitation generated there. These biases result in weaker correlation in vertical
555 winds between the reanalysis and the GFS forecasts with coefficients of 0.29 and 0.32 for 0.5°
556 and 1.0° resolutions, respectively. The MPAS experiment at 60 km simulates the vertical
557 motion toward the south around 28°N. The MPAS experiments at 30 km and 16 km generally
558 agree well with the ERA5 reanalysis, although both generate higher vertical motion in the south
559 (e.g. 25°N) to some extent. The correlation coefficients between the reanalysis and the MPAS
560 experiments at 60 km, 30 km, and 16 km are 0.53, 0.68, and 0.80, respectively. The MPAS
561 experiment at 4 km with the WSM6 scheme produces consistent vertical motion with that in
562 the ERA5 reanalysis, while the one with the Thompson scheme shifts the vertical motion a
563 little further north. Both experiments at 4 km have the highest correlation in the distributions
564 of vertical motion with the reanalysis with coefficients of 0.85 and 0.80 for WSM6 and
565 Thompson, respectively. The statistical significance tests based on the bootstrap analysis
566 indicate that at the 95% confidence level the model performance at 16 km and 4 km in terms
567 of simulating vertical structure of winds are comparable and better than the simulations at
568 coarser resolution (Table 2). The zonal distributions of precipitation discussed above
569 correspond well with the distributions of vertical motion in all the experiments. Differences in
570 the spatial distribution of vertical motions suggest that model resolution, and in some degree
571 cloud microphysics parameterizations, have important effects on simulating the structure of the

Deleted: ERA-interim

Deleted: ERA-interim

Deleted: 25

Deleted: 22

Deleted: ERA-interim

Deleted: 57

Deleted: 76

Deleted: ERA-interim

Deleted: 81 for WSM6 and Thompson, respectively.

581 wind shear over East China during the East Asian summer monsoon and the embedded
582 precipitation.

Deleted: Meiyu front

583

584 3.2.3 Distribution of extreme precipitation

585 Besides predicting the spatial and temporal variations of the rain belt, it is also critical
586 to capture the location and intensity of extreme precipitation within the heavy rain belt. Since
587 the GFS forecasts shift the entire rain belt northward, only the MPAS simulations are analyzed
588 here. Figure 10 shows the spatial distributions of precipitation averaged during the event over
589 the heavy rain region (27°N-32°N and 110°E-122°E). The CMA observations show that heavy
590 precipitation exceeding 50 mm/day mainly occurs over the plains of South Anhui province and
591 Southeast Hubei province and part of the Huang Mountains. The MPAS experiment at 60 km
592 simulates much smaller areas with heavy precipitation exceeding 50 mm/day. In addition, it
593 simulates heavy precipitation over some areas of Hunan province, which is not observed by
594 the CMA stations. The experiment at 30 km produces more numerous areas with heavy
595 precipitation and captures the locations of heavy precipitation over the Huang Mountains.
596 However, it misses the heavy precipitation over the plains of South Anhui province and
597 Southeast Hubei province; instead, it produces heavy precipitation over large areas of
598 mountainous regions over Hunan and Jiangxi provinces. The experiment at 16 km simulates
599 better spatial distribution of heavy precipitation, particularly capturing the heavy precipitation
600 over the Huang Mountains and the plain of South Anhui province, although it still shifts the
601 heavy precipitation from Southeast Hubei province to Hunan province. The experiments at 4
602 km are affected by the cloud microphysics. The 4 km experiment with the WSM6 scheme
603 produces the best spatial distribution among the MPAS experiments. It generally captures the
604 observed heavy precipitation areas during this event as discussed above, although the locations
605 do not perfectly match that of the observations. On the other hand, the 4 km experiment with
606 the Thompson microphysics produces more areas of heavy precipitation over Central Anhui
607 province. As a result, the correlation coefficients between the observations and the MPAS
608 experiments at the resolutions of 60 km, 30 km, 16 km, and 4 km are 0.20, 0.21, 0.29, 0.50
609 (WSM6), and 0.42 (Thompson), respectively. The statistical significance test based on the
610 bootstrap analysis indicates that at the 95% confidence level the simulations at 4 km can better
611 capture the spatial distribution of heavy precipitation than the simulations at resolutions of
612 hydrostatic scale (Table 2).

Deleted: reproduces

615 Figure 11 shows the probability density functions (PDFs) of hourly precipitation at all
616 the CMA stations during the event. Precipitation above ~5 mm/hour (~120 mm/day) is
617 considered very heavy and extra heavy storm rain event (refer to the CMA definition) that may
618 cause dramatic flooding and damage locally or regionally. During this event, for precipitation
619 lower than ~5 mm/hour, the MPAS simulations at hydrostatic scales (60 km, 30 km, and 16
620 km) overestimate the frequency, while above ~5 mm/hour, these simulations significantly
621 underestimate the frequency. In contrast, the MPAS simulations at convection-permitting scale
622 (4 km) produce much higher frequency of extreme precipitation above ~5 mm/hour, more
623 consistent with the observations. However, the simulated frequency of extreme precipitation at
624 convection-permitting scale depends on the cloud microphysics schemes. The Thompson
625 scheme produces much higher frequency than the WSM6 scheme and results in a positive bias
626 relative to the observations during this event, which deserves further investigation in future.
627 The results also indicate that the convective parameterization appears not to be able to produce
628 the higher intensity precipitation.

629 Previous studies found that the distribution of extreme precipitation correlates well with
630 that of the lower tropospheric upward vertical velocity (e.g., Zhao et al., 2016). Figure 12 shows
631 the PDFs of hourly upward vertical velocity averaged below 700 hPa at all the CMA stations
632 during the event from the MPAS simulations. In general, the comparison of lower-level upward
633 vertical velocity among the experiments is consistent with that of precipitation (Fig. 11) in that
634 simulations at hydrostatic scales (i.e., 60 km, 30 km, and 16 km in this study) produce higher
635 frequencies of updrafts < 4 cm/s than simulations at 4 km and vice versa for stronger updrafts.
636 The difference in updrafts between the 4 km MPAS simulations with two different cloud
637 microphysics schemes is negligible. Another analysis with the simulated updrafts at various
638 resolutions all regridded to 0.5° resolution shows the similar PDFs as Fig. 12. Previous studies
639 have proposed some mechanisms underlying the resolution impacts on modeling vertical
640 velocity (e.g., Rauscher et al., 2016; Jeevanjee et al., 2017; Herrington and Reed, 2017;
641 O'Brien et al., 2016; Fildier et al., 2018). Among these mechanisms, Rauscher et al. (2016)
642 argued that the resolution-dependent vertical velocity is caused by the interaction between the
643 constraint of fluid continuity and macro-scale turbulence. They suggested that the vertical
644 velocity should be more intense at higher resolution because the horizontal velocity increment
645 follows approximately a power law of resolution. Therefore, the resolved vertical transport
646 must increase as grid spacing decreases. Assuming atmospheric moisture is relatively

Formatted: Don't adjust right indent when grid is defined,
Don't adjust space between Latin and Asian text, Don't adjust
space between Asian text and numbers

insensitive to resolution, the upward moisture flux should increase as grid spacing decreases, hence producing more precipitation.

Formatted: Font color: Text 1

Figure 13 shows the PDFs of the upward moisture flux and the relationship between hourly precipitation versus upward moisture flux at 850hPa during the event from the MPAS simulations at 60km, 30km, 16km and 4km. It is evident that the simulations at higher resolutions produce more frequent intense upward moisture fluxes at 850hPa, consistent with Rauscher et al. (2016) and O'Brien et al. (2016). Rauscher et al. (2016) found a linear relationship between precipitation and upward moisture fluxes at lower level. The relationship lines from this study as shown in Fig. 13 parallel the 1:1 reference line for all resolutions. However, the lines are consistently below the reference line for the convection-permitting simulations (4km) and are above the reference line for the hydrostatic simulations with convective parameterization (e.g., 16km, 30km, 60km). The simulated precipitation can be larger than the lower level upward moisture fluxes at hydrostatic scale because part of the precipitation is contributed by the convective parameterization rather than contributed by the resolved upward moisture flux (Rauscher et al., 2016). On the contrary, precipitation could be lower than the upward moisture flux at convection-permitting scale (e.g., 4km) as moisture is removed from cloud updrafts due to detrainment (e.g., O'Brien et al., 2016). Overall, our results of the resolution-dependent updraft and precipitation are consistent with Rauscher et al. (2016) and O'Brien et al. (2016).

4. Summary and discussion

In this study, a series of MPAS simulations of a heavy precipitation event over East China, triggered by a typical southwest vortex in the middle and high troposphere and wind shear in the lower layer of the Meiyu front during the East Asian summer monsoon, are compared. The simulations are performed at various resolutions from hydrostatic (60 km, 30 km, 16 km) to non-hydrostatic (4 km) scales. Consistency between the MPAS simulations at global uniform and variable resolutions is also investigated. Besides the impacts of resolution on simulating heavy precipitation, the impacts of convective and cloud microphysics schemes are also examined. All the MPAS simulations are evaluated using the CMA station observations of precipitation and the ERA5 reanalysis of winds, and compared against the NCEP GFS forecasts that share the same initial condition of the MPAS simulations.

Deleted: are analyzed. The consistency

Deleted: ERA-interim

In general, the MPAS simulations at global uniform (U15km) and variable (V16km) resolutions produce similar results in terms of the spatial and temporal distributions of

precipitation and winds inside the refined region over East China. Both experiments can capture the observed precipitation characteristics. This suggests that the global variable-resolution configuration of MPAS may be appropriate to simulate heavy precipitation over East China, which is also consistent with the finding from previous studies using variable resolution MPAS with regional refinement over other parts of the globe (e.g., Sakaguchi et al., 2015; Zhao et al., 2016). The simulations with two different convective parameterizations show that the MPAS simulated distributions of precipitation are affected by the convective schemes at hydrostatic scales, while the impacts from the cloud microphysics schemes are small.

Deleted: the

Further investigation of MPAS experiments at multiple resolutions from hydrostatic (60 km, 30 km, 16 km) to non-hydrostatic (4 km) scales over East China shows significant impacts of resolution on simulating the spatial distributions of precipitation and winds. The variable-resolution simulations spanning hydrostatic and non-hydrostatic scales reveal that the scale-aware GF convective parameterization produces less convective parameterized precipitation as the horizontal resolution increases. Meanwhile, the subgrid-scale motions become increasingly resolved and the ratio of grid-scale to total precipitation increases over the refined region as resolution increases to 4 km. Comparison against the station observations indicates that the MPAS simulations at 16 km and 4 km can generally better capture the observed temporal and zonal distribution of the rain belt in the simulated event than the simulations at coarser resolutions. The simulations at coarser resolutions of 60 km and 30 km produce weaker precipitation and a southward shift of the rain belt. In contrast, the GFS forecasts at 0.5° and 1.0° produce a northward shift of the rain belt. The analysis also indicates the significant impacts from cloud microphysics on the MPAS simulations at 4 km in terms of precipitation distribution and intensity. The biases in the locations of rain belt are mainly due to failure of the model to simulate the wind shear structure of the Meiyu front during this event. The distributions of rain belt are consistent with the zonal shift of vertical motion. This suggests that the position and structure of the wind shear of the Meiyu front that produces the vertical motion is sensitive to the models and their specific configurations even though all simulations share the same initial condition. Previous studies have found that the formation and evolution of wind shear during the Meiyu front can interact with multiscale processes and systems over East China, including terrain and convective latent heat (Yao et al., 2017). Therefore, different representation of the terrain over East China in various resolutions and convective latent heat resulted from different physics schemes may affect the simulated wind shear structure among the MPAS experiments at various resolutions and between MPAS and GFS.

Deleted: (not shown).

Deleted: well

Moved (insertion) [1]

Deleted: The biases in the locations

Moved up [1]: The analysis also indicates the significant impacts from cloud microphysics on the MPAS simulations at 4 km in terms of precipitation distribution and intensity.

Formatted: Font color: Auto

722 Besides the general zonal distribution of the rain belt, the distribution and intensity of
 723 heavy precipitation are also investigated. The experiments at 4 km can better capture the areas
 724 with heavy precipitation (> 50 mm/day) than the experiments at coarser resolutions compared
 725 to the observations, although the simulations at 4 km overestimate the first peak precipitation
 726 and underestimate the second one. In addition, the MPAS simulations at 4 km can better
 727 generate the frequency of intense precipitation that is significantly underestimated by
 728 simulations at coarser resolutions, which may indicate that the convective parameterization
 729 appears not to be able to produce intense precipitation. The analysis also shows that the
 730 underestimation of intense precipitation is consistent with the underestimation of resolved
 731 upward motions in the simulations at coarser resolutions. Although the MPAS simulations at
 732 4 km generally produce better results than the experiments at coarser resolutions particularly
 733 30 km and up, they still have some biases in the timing and intensity of precipitation. In addition,
 734 the performance of MPAS at convection-permitting scale is quite sensitive to the cloud
 735 microphysics scheme in terms of the distribution and intensity of extreme precipitation. This
 736 is consistent with Feng et al. (2018), who found that cloud microphysics parameterizations in
 737 convection permitting regional simulations have important effects on macroscale properties
 738 such as the lifetime, precipitation amount, stratiform versus convective rain volumes of
 739 mesoscale convective systems in the U.S. They attributed the impacts to the representation of
 740 ice phase hydrometeor species that influence the mesoscale convective systems through their
 741 influence on the diabatic heating profiles that provide dynamical feedback to the circulation
 742 (Yang et al. 2017). Hence more efforts may be needed to improve cloud microphysics
 743 processes for modeling extreme precipitation at convection-permitting scale in the future. In
 744 the meantime, aerosols have been found to play a critical role in simulating some heavy
 745 precipitation events over China through their impacts on cloud microphysics and/or radiation
 746 (e.g., Zhong et al., 2015, 2017; Fan et al., 2015). The current version of MPAS does not
 747 represent aerosol-radiation and aerosol-cloud interactions, which may also contribute to the
 748 biases of extreme precipitation at convection-permitting scales. Lastly, it is also noteworthy
 749 that the resolution of 4 km may still be insufficient to resolve some convective cells, which
 750 may also contribute to the modeling biases (Bryan and Morrison, 2012).

751 This study provides the first evidence supporting the use of global variable resolution
 752 configuration of MPAS for simulating extreme precipitation events over East China. In
 753 particular, the MPAS variable-resolution experiment at convection-permitting scale (4 km)
 754 improves the simulated distribution and intensity of precipitation over the area of interest,
 755 which is consistent with previous studies using regional convection permitting models (e.g.,

Deleted: Among the MPAS

Deleted: with multiple resolutions, only the simulations

Deleted: observed locations of

Deleted: . All

Deleted: miss some areas of heavy

Deleted: or produce heavy precipitation in areas different from that observed.

Deleted: only

Deleted: reasonable

Deleted: .

Deleted: the best

Deleted: among

Deleted: various

Deleted: well

Zhang et al., 2013; Prein et al., 2015; Yang et al. 2017; Gao et al. 2017; Feng et al. 2018). The higher resolution MPAS experiments simulate better spatial distribution of heavy precipitation over the complex topographic region of East China, which suggests that topography may play a critical role and deserves further investigation in the future. Our results show that cloud microphysics parameterizations have important effects in convection permitting simulations, but modeling of other physical processes such as boundary layer turbulence, radiation, and aerosols may also affect the skill of convection permitting simulations. The GFS forecasts analyzed in this study show significant biases in precipitation distribution. The zonal shift of the rain belt by the MPAS simulations at coarser resolutions compared to simulations at finer resolutions suggests that resolution may have contributed to the GFS forecast biases. A more detailed exploration of the differences between the MPAS and GFS simulations is beyond the scope of this study.

Previous studies (Xue et al., 2007; Clark et al. 2016) noted the importance of ensemble simulations in predicting heavy precipitation. Due to the computational limitation, only one set of experiments with different physics and resolutions are evaluated in this study. The MPAS simulations of heavy precipitation with different initial conditions and refinement sizes deserve more evaluations. Finally, some studies noted that convection-permitting modeling does not always add values in simulating heavy precipitation compared to hydrostatic scale modeling (e.g., Kain et al., 2008; Rhoades et al., 2018; Xu et al., 2018). Rhoades et al. (2018) found that the improvement by increasing resolution may also depend on cloud microphysics parameterization. Increasing horizontal resolution alone sometimes can even lead to worse model performance. The impacts of increasing horizontal resolution on the overall model performance in simulating extreme precipitation may also be affected by the model structure and coupling among model components and processes (Jeevanjee et al., 2016; O'Brien et al., 2016; Herrington et al., 2017, 2018; Gross et al., 2018). This study also found some sensitivity of modeling extreme precipitation to cloud microphysics, particularly at convection-permitting scale. More events of heavy precipitation over East China should be investigated in the future to more systematically evaluate the MPAS variable-resolution modeling framework and the impacts of resolution and physical parameterizations.

799

Code availability

The MPAS release v5.2 can be obtained at *mpas-dev.github.io*. Global meshes generated for the experiments used in this study are available upon request by contacting the corresponding author.

Moved (insertion) [2]

Deleted: Although the

Deleted: , some GFS forecasts initialized at different times are found to produce more reasonable results (not shown), supporting the need for ensemble modeling for forecasting extreme events. However, the

Formatted: Indent: First line: 1.27 cm

Deleted: .

Moved up [2]: Our results show that cloud microphysics parameterizations have important effects in convection permitting simulations, but modeling of other physical processes such as boundary layer turbulence, radiation, and aerosols may also affect the skill of convection permitting simulations.

Deleted: Furthermore, more

817
818
819
820
821
822
823
824
825
826
827
828
829
830
831
832

Author contributions

CZ and YW designed research. MX performed the simulations. CZ, MX, MZ, and ZH analyzed the simulations. JG collected and analyzed the observations. CZ, MX, and YW wrote the paper. LRL, MD, and WS guided the experiment design and edited the paper.

Acknowledgements

This research was supported by the Ministry of Science and Technology of China under grant 2017YFC1501401, and the Fundamental Research Funds for the Central Universities. The study used computing resources from the High-Performance Computing Center of University of Science and Technology of China (USTC) and the TH-2 of National Supercomputer Center in Guangzhou (NSCC-GZ). Leung was supported by the U.S. Department of Energy Office of Science Biological and Environmental Research as part of the Regional and Global Modeling and Analysis program. PNNL is operated for the Department of Energy under contract DE-AC05-76RL01830.

Deleted: , the Thousand Talents Plan for Young Professionals, the
Deleted: , and the National Natural Science Foundation of China (grant 41775146).

837 **Reference**

- 838 Arakawa, A., Jung, J. H., & Wu, C. M.: Toward unification of the multiscale modeling of the
839 atmosphere. *Atmospheric Chemistry and Physics*, 11(8), 3731-3742.
840 <https://doi.org/10.5194/acp-11-3731-2011>, 2011.
- 841 Bacmeister, J. T., Wehner, M. F., Neale, R. B., Gettelman, A., Hannay, C., Lauritzen, P. H., ...
842 & Truesdale, J. E.: Exploratory high-resolution climate simulations using the
843 Community Atmosphere Model (CAM). *Journal of Climate*, 27(9), 3073-3099.
844 <https://doi.org/10.1175/JCLI-D-13-00387.1>, 2014.
- 845 Bechtold, P., Chaboureaud, J. P., Beljaars, A., Betts, A. K., Köhler, M., Miller, M., &
846 Redelsperger, J. L.: The simulation of the diurnal cycle of convective precipitation over
847 land in a global model. *Quarterly Journal of the Royal Meteorological*
848 *Society*, 130(604), 3119-3137. <https://doi.org/10.1256/qj.03.103>, 2004.
- 849 Bechtold, P., Köhler, M., Jung, T., Doblas-Reyes, F., Leutbecher, M., Rodwell, M. J., ... &
850 Balsamo, G.: Advances in simulating atmospheric variability with the ECMWF model:
851 From synoptic to decadal time-scales. *Quarterly Journal of the Royal Meteorological*
852 *Society*, 134(634), 1337-1351. <https://doi.org/10.1002/qj.289>, 2008.
- 853 Bechtold, P., Semane, N., Lopez, P., Chaboureaud, J. P., Beljaars, A., & Bormann, N.:
854 Representing equilibrium and nonequilibrium convection in large-scale
855 models. *Journal of the Atmospheric Sciences*, 71(2), 734-753.
856 <https://doi.org/10.1175/JAS-D-13-0163.1>, 2014.
- 857 Bryan, G. H., and H. Morrison: Sensitivity of a simulated squall line to horizontal resolution
858 and parameterization of microphysics. *Mon. Wea. Rev.*, 140, 202-225,
859 <https://doi.org/10.1175/MWR-D-11-00046.1>, 2012.
- 860 Burakowski, E. A., Tawfik, A., Ouimette, A., Lepine, L., Zarzycki, C., Novick, K., ... & Bonan,
861 G.: Simulating surface energy fluxes using the variable-resolution Community Earth
862 System Model (VR-CESM). *Theoretical and Applied Climatology*, 1-19.
863 <https://doi.org/10.1007/s00704-019-02785-0>, 2019.
- 864 Chauvin, F., J.-F. Royer, and M. Deque: Response of hurricane type vortices to global warming
865 as simulated by ARPEGE-Climat at high resolution. *Climate Dyn.*, 27, 377-399,
866 <https://doi.org/10.1007/s00382-006-0135-7>, 2006.
- 867 Chen, F., & Dudhia, J.: Coupling an advanced land surface-hydrology model with the Penn
868 State-NCAR MM5 modeling system. Part I: Model implementation and

Deleted: . (2011):

Deleted: <https://doi.org/10.5194/acp-11-3731-2011>

Deleted: . (2014):

Deleted: . (2004):

Deleted: . (2008):

Deleted: . (2014):

Deleted: .

Deleted: , 2012

Deleted: <https://doi.org/10.1175/MWR-D-11-00046.1>

Formatted: Hyperlink, Font:+Theme Body (Calibri)

Deleted: (2006):

Deleted: doi:10.1007/s00382-006-0135-7

Deleted: . (2001):

881 sensitivity. Monthly Weather Review, 129(4), 569-585. [https://doi.org/10.1175/1520-0493\(2001\)129<0569:CAALSH>2.0.CO;2](https://doi.org/10.1175/1520-0493(2001)129<0569:CAALSH>2.0.CO;2), 2001.

882

883 Déqué, M., Jones, R. G., Wild, M., Giorgi, F., Christensen, J. H., Hassell, D. C., ... & De Castro, M.: Global high resolution versus Limited Area Model climate change projections over Europe: quantifying confidence level from PRUDENCE results. Climate Dynamics, 25(6), 653-670. <https://doi.org/10.1007/s00382-005-0052-1>, 2005.

884

885

886

887 Déqué, M., & Piedelievre, J. P.: High resolution climate simulation over Europe. Climate dynamics, 11(6), 321-339. <https://doi.org/10.1007/BF00215735>, 1995.

888

889 Déqué, M., Rowell, D. P., Lüthi, D., Giorgi, F., Christensen, J. H., Rockel, B., ... & van den Hurk, B. J. J. M.: An intercomparison of regional climate simulations for Europe: assessing uncertainties in model projections. Climatic Change, 81(1), 53-70. <https://doi.org/10.1007/s10584-006-9228-x>, 2007.

890

891

892

893 Ding, Y., Wang, Z., & Sun, Y.: Inter-decadal variation of the summer precipitation in East China and its association with decreasing Asian summer monsoon. Part I: Observed evidences. International Journal of Climatology, 28(9), 1139-1161. <https://doi.org/10.1002/joc.1615>, 2008.

894

895

896

897 Clark, P., Roberts, N., Lean, H., Ballard, S. P., & Charlton-Perez, C.: Convection-permitting models: a step-change in rainfall forecasting. Meteorological Applications, 23(2), 165-181. <https://doi.org/10.1002/met.1538>, 2016.

898

899

900 Du, Q., Faber, V., & Gunzburger, M.: Centroidal Voronoi tessellations: Applications and algorithms. SIAM review, 41(4), 637-676. <https://doi.org/10.1137/S0036144599352836>, 1999.

901

902

903 ECMWF: ECMWF strategy 2016–2025: The strength of a common goal. European Centre for Medium-Range Weather Forecasts Tech. Rep., 32 pp. https://www.ecmwf.int/sites/default/files/ECMWF_Strategy_2016-2025.pdf, 2016.

904

905

906 Efron, B.: Bootstrap methods: another look at the jackknife. In Breakthroughs in statistics (pp. 569-593). Springer, New York, NY. https://doi.org/10.1007/978-1-4612-4380-9_41, 1992.

907

908

909 Efron, B., & Tibshirani, R. J.: An introduction to the bootstrap. CRC press, 1994.

910

911 Fan, J., Rosenfeld, D., Yang, Y., Zhao, C., Leung, L. R., & Li, Z.: Substantial contribution of anthropogenic air pollution to catastrophic floods in Southwest China. Geophysical Research Letters, 42(14), 6066-6075. <https://doi.org/10.1002/2015GL064479>, 2015.

912

Moved down [3]: M.,
 Deleted: Dee, D. P., Uppala, S.
 Deleted: Simmons, A. J., Berrisford,
 Moved down [4]: P.,
 Deleted: Poli, P., Kobayashi, S., ... & Bechtold, P. (2011): The ERA- Interim reanalysis: Configuration and performance of the data assimilation system. Quarterly Journal of the royal meteorological society, 137(656). <https://doi.org/10.1002/qj.828> .
 Deleted: . (2005):
 Deleted: <https://doi.org/10.1007/s00382-005-0052-1>
 Deleted: . (1995):
 Deleted: <https://doi.org/10.1007/BF00215735>
 Deleted: . (2007):
 Deleted: <https://doi.org/10.1007/s10584-006-9228-x>
 Deleted: . (2008):

Moved (insertion) [4]

Deleted: . (1999):

Deleted: . (2016):

Deleted: .

Deleted: . (2015):

933 Feng, Z., L.R. Leung, R.A. Houze, Jr., S. Hagos, J. Hardin, Q. Yang, B. Han, & J. Fan:
 934 Structure and evolution of mesoscale convective systems: sensitivity to cloud
 935 microphysics in convection-permitting simulations over the U.S. J. Adv. Model. Earth
 936 Syst., 10, <https://doi.org/10.1029/2018MS001305>, 2018.

937 Fowler, L. D., Skamarock, W. C., Grell, G. A., Freitas, S. R., & Duda, M. G.: Analyzing the
 938 Grell–Freitas convection scheme from hydrostatic to nonhydrostatic scales within a
 939 global model. Monthly Weather Review, 144(6), 2285-2306.
 940 <https://doi.org/10.1175/MWR-D-15-0311.1>, 2016.

941 Fritsch, J. M., & Carbone, R. E.: Improving quantitative precipitation forecasts in the warm
 942 season: A USWRP research and development strategy. Bulletin of the American
 943 Meteorological Society, 85(7), 955-966. <https://doi.org/10.1175/BAMS-85-7-955>,
 944 2004.

945 Gao, Y., L.R. Leung, C. Zhao, & S. Hagos: Sensitivity of summer precipitation to model
 946 resolution and convective parameterizations across gray zone resolutions. J. Geophys.
 947 Res., 122, 2714-2733, doi:10.1002/2016JD025896, 2017.

948 Gettelman, A., Callaghan, P., Larson, V. E., Zarzycki, C. M., Bacmeister, J. T., Lauritzen, P.
 949 H., ... & Neale, R. B.: Regional climate simulations with the community earth system
 950 model. Journal of Advances in Modeling Earth Systems, 10(6), 1245-1265.
 951 <https://doi.org/10.1002/2017MS001227>, 2018.

952 Gettelman A., Morrison H., Thompson G.: Cloud Microphysics Across Scales for Weather and
 953 Climate. In: Randall D., Srinivasan J., Nanjundiah R., Mukhopadhyay P. (eds) Current
 954 Trends in the Representation of Physical Processes in Weather and Climate Models.
 955 Springer Atmospheric Sciences. Springer, Singapore, 2019.

956 Giorgi, F., and Marinucci, M. R.: A investigation of the sensitivity of simulated precipitation
 957 to model resolution and its implications for climate studies. Monthly Weather
 958 Review, 124(1), 148-166. [https://doi.org/10.1175/1520-0493\(1996\)124<0148:AIOTSO>2.0.CO;2](https://doi.org/10.1175/1520-0493(1996)124<0148:AIOTSO>2.0.CO;2), 1996.

960 Giorgi, F., and Mearns, L. O.: Approaches to the simulation of regional climate change: a
 961 review. Reviews of Geophysics, 29(2), 191-216. <https://doi.org/10.1029/90RG02636>,
 962 1991.

963 Grell, G. A., & Dévényi, D.: A generalized approach to parameterizing convection combining
 964 ensemble and data assimilation techniques. Geophysical Research Letters, 29(14), 38-
 965 1. <https://doi.org/10.1029/2002GL015311>, 2002.

Deleted: (2018):

Deleted: doi: 10.1029/2018MS001305

Deleted: . (2016):

Deleted: Fox-Rabinovitz, M., Côté, J., Dugas, B., Déqué,

Moved down [5]: M.,

Deleted: & McGregor, J. L. (2006): Variable resolution
 general circulation models: Stretched grid model
 intercomparison project (SGMIP). Journal of Geophysical
 Research: Atmospheres, 111(D16).
<https://doi.org/10.1029/2005JD006520> .

[1]

Moved down [6]: J.,

Deleted: & Takacs, L. L. (1997): A finite-difference GCM
 dynamical core with a variable-resolution stretched
 grid. Monthly Weather Review, 125(11), 2943-2968.
[https://doi.org/10.1175/1520-0493\(1997\)125<2943:AFDGDG>2.0.CO;2](https://doi.org/10.1175/1520-0493(1997)125<2943:AFDGDG>2.0.CO;2) .

Deleted: . (2004):

Deleted: .

Deleted: (2017):

Moved (insertion) [3]

Moved (insertion) [7]

Deleted: &

Deleted: . (1996):

Deleted: &

Deleted: . (1991):

Deleted: . (2002):

991	Grell, G. A., & Freitas, S. R.: A scale and aerosol aware stochastic convective parameterization	Deleted: . (2014):
992	for weather and air quality modeling. Atmos. Chem. Phys, 14(10), 5233-5250.	
993	https://doi.org/10.5194/acp-14-5233-2014 , 2014.	Deleted: .
994	Gross, M., Wan, H., Rasch, P. J., Caldwell, P. M., Williamson, D. L., Klocke, D., Christiane,	Moved (insertion) [6]
995	J, Diana, T., Nigel, W., Mike, C, Bob, B., Martin, W., Florian, L., Eric, B., Sylvie, M.,	Moved (insertion) [5]
996	Piet, T., Almut, G., Peter, L., Hans, J., Colin, Z., Sakaguchi, K., Leung, R.: Physics–	
997	Dynamics Coupling in Weather, Climate, and Earth System Models: Challenges and	
998	Recent Progress. Monthly Weather Review, 146(11), 3505-3544.	
999	https://doi.org/10.1175/MWR-D-17-0345.1 , 2018.	
1000	Guo, J., Su, T., Li, Z., Miao, Y., Li, J., Liu, H., Xu, H., Cribb, M., and Zhai, P.: Declining	Deleted: . &
1001	frequency of summertime local-scale precipitation over eastern China from 1970 to	Deleted: . (2017):
1002	2010 and its potential link to aerosols. Geophysical Research Letters, 44(11), 5700–	
1003	5708, 2017.	
1004	Hagos, S., Leung, L. R., Yang, Q., Zhao, C., and Lu, J.: Resolution and dynamical core	Deleted: &
1005	dependence of atmospheric river frequency in global model simulations. Journal of	Deleted: . (2015):
1006	Climate, 28(7), 2764-2776. https://doi.org/10.1175/JCLI-D-14-00567.1 , 2015.	
1007	Herrington, A. R., & Reed, K. A.: An explanation for the sensitivity of the mean state of the	
1008	community atmosphere model to horizontal resolution on aquaplanets. Journal of	
1009	Climate, 30(13), 4781-4797. https://doi.org/10.1175/JCLI-D-16-0069.1 , 2017.	
1010	Herrington, A. R., & Reed, K. A.: An Idealized Test of the Response of the Community	
1011	Atmosphere Model to Near - Grid - Scale Forcing Across Hydrostatic	
1012	Resolutions. Journal of Advances in Modeling Earth Systems, 10(2), 560-575.	
1013	https://doi.org/10.1002/2017MS001078 , 2018.	
1014	Fildier, B., Parishani, H., & Collins, W. D.: Prognostic Power of Extreme Rainfall Scaling	
1015	Formulas Across Space and Time Scales. Journal of Advances in Modeling Earth	
1016	Systems, 10(12), 3252-3267. https://doi.org/10.1029/2018MS001462 , 2018.	
1017	Hong, S. Y.: A new stable boundary-layer mixing scheme and its impact on the simulated East	Deleted: . (2010):
1018	Asian summer monsoon. Quarterly Journal of the Royal Meteorological	
1019	Society, 136(651), 1481-1496. https://doi.org/10.1002/qj.665 , 2010.	
1020	Hong, S. Y., & Lim, J. O. J.: The WRF single-moment 6-class microphysics scheme	Deleted: . (2006):
1021	(WSM6). J. Korean Meteor. Soc, 42(2), 129-151, 2006.	Deleted: .

1031	Hong, S. Y., Noh, Y., & Dudhia, J.: A new vertical diffusion package with an explicit treatment	Deleted: . (2006):
1032	of entrainment processes. Monthly weather review, 134(9), 2318-2341.	
1033	https://doi.org/10.1175/MWR3199.1 , 2006.	
1034	Huang, X., Rhoades, A. M., Ullrich, P. A., & Zarzycki, C. M.: An evaluation of the variable-	Moved (insertion) [8]
1035	resolution CESM for modeling California's climate. Journal of Advances in Modeling	
1036	Earth Systems, 8(1), 345-369. https://doi.org/10.1002/2015MS000559 , 2016.	
1037	Hui, P., Tang, J., Wang, S., & Wu, J.: Sensitivity of simulated extreme precipitation and	Deleted: . (2015):
1038	temperature to convective parameterization using RegCM3 in China. Theoretical and	
1039	applied climatology, 122(1-2), 315-335. https://doi.org/10.1007/s00704-014-1300-2 ,	Deleted: https://doi.org/10.1007/s00704-014-1300-2
1040	2015.	
1041	Iacono, M. J., Mlawer, E. J., Clough, S. A., & Morcrette, J. J.: Impact of an improved longwave	Deleted: . (2000):
1042	radiation model, RRTM, on the energy budget and thermodynamic properties of the	
1043	NCAR community climate model, CCM3. Journal of Geophysical Research:	
1044	Atmospheres, 105(D11), 14873-14890. https://doi.org/10.1029/2000JD900091 , 2000.	Deleted: .
1045	Jeevanjee, N.: Vertical velocity in the gray zone. Journal of Advances in Modeling Earth	
1046	Systems, 9(6), 2304-2316. https://doi.org/10.1002/2017MS001059 , 2017.	
1047	Judt, F.: Insights into Atmospheric Predictability through Global Convection-Permitting Model	Deleted: . (2018):
1048	Simulations. Journal of the Atmospheric Sciences, 75(5), 1477-1497.	
1049	https://doi.org/10.1175/JAS-D-17-0343.1 , 2018.	
1050	Ju, L., Ringler, T., & Gunzburger, M.: Voronoi tessellations and their application to climate	Deleted: . (2011):
1051	and global modeling. In Numerical techniques for global atmospheric models (pp. 313-	
1052	342). Springer, Berlin, Heidelberg. https://doi.org/10.1007/978-3-642-11640-7_10 ,	
1053	2011.	
1054	Kain, J. S.: The Kain-Fritsch convective parameterization: an update. Journal of applied	Deleted: . (2004):
1055	meteorology, 43(1), 170-181. <a href="https://doi.org/10.1175/1520-0450(2004)043<0170:TKCPAU>2.0.CO;2">https://doi.org/10.1175/1520-0450(2004)043<0170:TKCPAU>2.0.CO;2 , 2004.	
1056	Kain, J. S., Weiss, S. J., Bright, D. R., Baldwin, M. E., Levit, J. J., Carbin, G. W., ... & Thomas,	
1057	K. W.: Some practical considerations regarding horizontal resolution in the first	Deleted: . (2008):
1058	generation of operational convection-allowing NWP. Weather and Forecasting, 23(5),	
1059	931-952. https://doi.org/10.1175/WAF2007106.1 , 2008.	Deleted: .
1060	Klemp, J. B.: A terrain-following coordinate with smoothed coordinate surfaces. Monthly	Deleted: . (2011):
1061	weather review, 139(7), 2163-2169. https://doi.org/10.1175/MWR-D-10-05046.1 ,	Deleted: https://doi.org/10.1175/MWR-D-10-05046.1
1062	2011.	
1063		

1076	Klemp, J. B., Skamarock, W. C., & Dudhia, J.: Conservative split-explicit time integration	Deleted: . (2007):
1077	methods for the compressible nonhydrostatic equations. Monthly Weather	
1078	Review, 135(8), 2897-2913. https://doi.org/10.1175/MWR3440.1 , 2007.	
1079	Landu, K., Leung, L. R., Hagos, S., Vиноj, V., Rauscher, S. A., Ringler, T., & Taylor, M.: The	Deleted: . (2014):
1080	dependence of ITCZ structure on model resolution and dynamical core in aquaplanet	
1081	simulations. Journal of Climate, 27(6), 2375-2385. https://doi.org/10.1175/JCLI-D-13-	
1082	00269.1, 2014.	
1083	Laprise, R.: Regional climate modelling. Journal of Computational Physics, 227(7), 3641-3666.	Deleted: . (2008):
1084	https://doi.org/10.1016/j.jcp.2006.10.024 , 2008.	
1085	Leung, L. R., & Qian, Y.: The sensitivity of precipitation and snowpack simulations to model	Deleted: . (2003):
1086	resolution via nesting in regions of complex terrain. Journal of Hydrometeorology, 4(6),	
1087	1025-1043. <a href="https://doi.org/10.1175/1525-7541(2003)004<1025:TSOPAS>2.0.CO;2">https://doi.org/10.1175/1525-7541(2003)004<1025:TSOPAS>2.0.CO;2 ,	
1088	2003.	
1089	Leung, L. R., Ringler, T., Collins, W. D., Taylor, M., & Ashfaq, M.: A hierarchical evaluation	
1090	of regional climate simulations. Eos, Transactions American Geophysical	
1091	Union, 94(34), 297-298. https://doi.org/10.1002/2013EO340001, 2013.	
1092	Li, J., Zhang, Q., Chen, Y. D., & Singh, V. P.: GCMssimulations. Eos, Transactions American	Deleted: . (2013): GCMs-based spatiotemporal evolution of climate
1093	Ge extremes during the 21st century in China. Journal of Geophysical Research:	
1094	Atmospheres, 118(19). https://doi.org/10.1002/jgrd.50851, 2013.	Deleted: .
1095	Li, W., Jiang, Z., Xu, J., & Li, L.: Extreme Precipitation Indices over China in CMIP5 Models.	Deleted: . (2016):
1096	Part II: Probabilistic Projection. Journal of Climate, 29(24), 8989-9004.	
1097	https://doi.org/10.1175/JCLI-D-16-0377.1 , 2016.	Deleted: .
1098	Li, Z., W. K.-M. Lau, V. Ramanathan et al.: Aerosol and monsoon climate interactions over	Deleted: . (2016):
1099	Asia, <i>Rev. Geophys.</i> , 54, https://doi.org/10.1002/2015RG000500 , 2016.	Deleted: doi:10.1002/2015RG000500
1100	Lin, Z., & Wang, B.: Northern East Asian low and its impact on the interannual variation of	Formatted: Font: 12 pt
1101	East Asian summer rainfall. Climate dynamics, 46(1-2), 83-97.	Deleted: . (2016):
1102	https://doi.org/10.1007/s00382-015-2570-9 , 2016.	
1103	Liu, R., Liu, S. C., Cicerone, R. J., Shiu, C. J., Li, J., Wang, J., & Zhang, Y.: Trends of extreme	Deleted: . (2015):
1104	precipitation in eastern China and their possible causes. Advances in Atmospheric	
1105	Sciences, 32(8), 1027-1037. https://doi.org/10.1007/s00376-015-5002- , 2015.	Deleted: .
1106	Locatelli, J. D., & Hobbs, P. V.: Fall speeds and masses of solid precipitation particles. Journal	
1107	of Geophysical Research, 79(15), 2185-2197.	
1108	https://doi.org/10.1029/JC079i015p02185 , 1974.	

1123 Lorant, V., & Royer, J. F.: Sensitivity of equatorial convection to horizontal resolution in
 1124 aquaplanet simulations with a variable-resolution GCM. *Monthly weather*
 1125 *review*, 129(11), 2730-2745. [https://doi.org/10.1175/1520-](https://doi.org/10.1175/1520-0493(2001)129<2730:SOECTH>2.0.CO;2)
 1126 [0493\(2001\)129<2730:SOECTH>2.0.CO;2](https://doi.org/10.1175/1520-0493(2001)129<2730:SOECTH>2.0.CO;2), 2001.
 1127 Lu, J., Chen, G., Leung, L. R., Burrows, D. A., Yang, Q., Sakaguchi, K., & Hagos, S.: Toward
 1128 the dynamical convergence on the jet stream in aquaplanet AGCMs. *Journal of*
 1129 *Climate*, 28(17), 6763-6782. <https://doi.org/10.1175/JCLI-D-14-00761.1>, 2015.
 1130 Mlawer, E. J., Taubman, S. J., Brown, P. D., Iacono, M. J., & Clough, S. A.: Radiative transfer
 1131 for inhomogeneous atmospheres: RRTM, a validated correlated-k model for the
 1132 longwave. *Journal of Geophysical Research: Atmospheres*, 102(D14), 16663-16682.
 1133 <https://doi.org/10.1029/97JD00237>, 1997.
 1134 Molthan, A. L., & Colle, B. A.: Comparisons of single-and double-moment microphysics
 1135 schemes in the simulation of a synoptic-scale snowfall event. *Monthly Weather Review*,
 1136 140(9), 2982-3002. <https://doi.org/10.1175/MWR-D-11-00292.1>, 2012.
 1137 Nakanishi, M., & Niino, H.: An improved Mellor–Yamada level-3 model: Its numerical
 1138 stability and application to a regional prediction of advection fog. *Boundary-Layer*
 1139 *Meteorology*, 119(2), 397-407. <https://doi.org/10.1007/s10546-005-9030-8>, 2006.
 1140 Nakanishi, M., & Niino, H.: Development of an improved turbulence closure model for the
 1141 atmospheric boundary layer. *Journal of the Meteorological Society of Japan. Ser.*
 1142 *II*, 87(5), 895-912. <https://doi.org/10.2151/jmsj.87.895>, 2009.
 1143 NRC: National Research Council Board, *A National Strategy for Advancing Climate Modeli*
 1144 *ng*, The National Academies Press, Washington, DC (2012) ([http://www.nap.edu/cata](http://www.nap.edu/catalog/13430/a-national-strategy-for-advancing-climate-modeling)
 1145 [log/13430/a-national-strategy-for-advancing-climate-](http://www.nap.edu/catalog/13430/a-national-strategy-for-advancing-climate-modeling)
 1146 [modeling](http://www.nap.edu/catalog/13430/a-national-strategy-for-advancing-climate-modeling), last access: April 25, 2019).
 1147 O'Brien, T. A., Collins, W. D., Kashinath, K., Rübel, O., Byna, S., Gu, J., Krishnan, H., Ullrich,
 1148 P.: Resolution dependence of precipitation statistical fidelity in hindcast
 1149 simulations. *Journal of Advances in Modeling Earth Systems*, 8(2), 976-990.
 1150 <https://doi.org/10.1002/2016MS000671>, 2016.
 1151 O'Brien, T. A., Li, F., Collins, W. D., Rauscher, S. A., Ringler, T. D., Taylor, M., Hagos, S.
 1152 M., Leung, L. R.: Observed scaling in clouds and precipitation and scale incognizance
 1153 in regional to global atmospheric models. *Journal of Climate*, 26(23), 9313-9333.
 1154 <https://doi.org/10.1175/JCLI-D-13-00005.1>, 2013.

Deleted: . (2001):

Deleted: . (2015):

Deleted: Medvigy, D., Walko, R. L., Otte, M. J., & Avissar, R. (2013): Simulated changes in northwest US climate in response to Amazon deforestation. *Journal of Climate*, 26(22), 9115-9136. <https://doi.org/10.1175/JCLI-D-12-00775.1>

Deleted: . (1997):

Deleted: . (2006):

Deleted: . (2009):

Deleted: ... &

Deleted: . (2013):

1167 Park, S. H., Skamarock, W. C., Klemp, J. B., Fowler, L. D., & Duda, M. G.: Evaluation of
1168 global atmospheric solvers using extensions of the Jablonowski and Williamson
1169 baroclinic wave test case. *Monthly Weather Review*, 141(9), 3116-3129.
1170 <https://doi.org/10.1175/MWR-D-12-00096.1>, 2013.

1171 Pedersen, C. A., & Winther, J. G.: Intercomparison and validation of snow albedo
1172 parameterization schemes in climate models. *Climate Dynamics*, 25(4), 351-362:
1173 <https://doi.org/10.1007/s00382-005-0037-0>, 2005.

1174 Prein, A. F., Langhans, W., Fosser, G., Ferrone, A., Ban, N., Goergen, K., ... & Brisson, E.: A
1175 review on regional convection - permitting climate modeling: Demonstrations,
1176 prospects, and challenges. *Reviews of geophysics*, 53(2), 323-361.
1177 <https://doi.org/10.1002/2014RG000475>, 2015.

1178 Prein, A. F., Rasmussen, R. M., Ikeda, K., Liu, C., Clark, M. P., & Holland, G. J.: The future
1179 intensification of hourly precipitation extremes. *Nature Climate Change*, 7(1), 48.
1180 <https://doi.org/10.1038/nclimate3168>, 2017.

1181 Rauscher, S. A., O'Brien, T. A., Piani, C., Coppola, E., Giorgi, F., Collins, W. D., & Lawston,
1182 P. M.: A multimodel intercomparison of resolution effects on precipitation: simulations
1183 and theory. *Climate dynamics*, 47(7-8), 2205-2218. [https://doi.org/10.1007/s00382-](https://doi.org/10.1007/s00382-015-2959-5)
1184 [015-2959-5](https://doi.org/10.1007/s00382-015-2959-5), 2016.

1185 Rauscher, S. A., Ringler, T. D., Skamarock, W. C., & Mirin, A. A.: Exploring a global
1186 multiresolution modeling approach using aquaplanet simulations. *Journal of*
1187 *Climate*, 26(8), 2432-2452. <https://doi.org/10.1175/JCLI-D-12-00154.1>, 2013.

1188 Rhoades, A. M., Huang, X., Ullrich, P. A., & Zarzycki, C. M.: Characterizing Sierra Nevada
1189 snowpack using variable-resolution CESM. *Journal of Applied Meteorology and*
1190 *Climatology*, 55(1), 173-196. <https://doi.org/10.1175/JAMC-D-15-0156.1>, 2016.

1191 Rhoades, A. M., Ullrich, P. A., Zarzycki, C. M., Johansen, H., Margulis, S. A., Morrison, H., ...
1192 & Collins, W. D.: Sensitivity of Mountain Hydroclimate Simulations in Variable-
1193 Resolution CESM to Microphysics and Horizontal Resolution. *Journal of Advances in*
1194 *Modeling Earth Systems*, 10(6), 1357-1380. <https://doi.org/10.1029/2018MS001326>,
1195 2018.

1196 Ringler, T. D., Jacobsen, D., Gunzburger, M., Ju, L., Duda, M., & Skamarock, W.: Exploring
1197 a multiresolution modeling approach within the shallow-water equations. *Monthly*
1198 *Weather Review*, 139(11), 3348-3368. <https://doi.org/10.1175/MWR-D-10-05049.1>,
1199 2011.

Deleted: . (2013):

Deleted: . (2005):

Deleted: <https://doi.org/10.1007/s00382-005-0037-0>

Deleted: . (2015):

Deleted: . (2017):

Deleted: <https://doi.org/10.1038/nclimate3168>

Deleted: . (2013):

Deleted: . (2011):

1208 1209 1210 1211 1212 1213 1214 1215 1216 1217 1218 1219 1220 1221 1222 1223 1224 1225 1226 1227 1228 1229 1230 1231 1232 1233 1234 1235 1236 1237 1238 1239 1240	Ringler, T., Ju, L., & Gunzburger, M.: A multiresolution method for climate system modeling: Application of spherical centroidal Voronoi tessellations. <i>Ocean Dynamics</i> , 58(5-6), 475-498. https://doi.org/10.1007/s10236-008-0157-2 , 2008. Sakaguchi, K., Leung, L. R., Zhao, C., Yang, Q., Lu, J., Hagos, S.: Exploring a multiresolution approach using AMIP simulations. <i>Journal of Climate</i> , 28(14), 5549-5574. https://doi.org/10.1175/JCLI-D-14-00729.1 , 2015. Sakaguchi, K., Lu, J., Leung, L. R., Zhao, C., Li, Y., & Hagos, S.: Sources and pathways of the upscale effects on the Southern Hemisphere jet in MPAS simulations. <i>Journal of Climate</i> , 29(10), 3090-3105. https://doi.org/10.1175/JCLI-D-14-00729.1 , 2016. Skamarock, W. C., & Gassmann, A.: Conservative transport schemes for spherical geodesic grids: High-order flux operators for ODE-based time integration. <i>Monthly Weather Review</i> , 139(9), 2962-2975. https://doi.org/10.1175/MWR-D-10-05056.1 , 2011. Skamarock, W. C., & Klemp, J. B.: A time-split nonhydrostatic atmospheric model for weather research and forecasting applications. <i>Journal of Computational Physics</i> , 227(7), 3465-3485. https://doi.org/10.1016/j.jcp.2007.01.037 , 2008. Skamarock, W. C., Klemp, J. B., Duda, M. G., Fowler, L. D., Park, S. H., & Ringler, T. D.: A multiscale nonhydrostatic atmospheric model using centroidal Voronoi tessellations and C-grid staggering. <i>Monthly Weather Review</i> , 140(9), 3090-3105. https://doi.org/10.1175/MWR-D-11-00215.1 , 2012. Sukovich, E. M., Ralph, F. M., Barthold, F. E., Reynolds, D. W., & Novak, D. R.: Extreme quantitative precipitation forecast performance at the Weather Prediction Center from 2001 to 2011. <i>Weather and Forecasting</i> , 29(4), 894-911. https://doi.org/10.1175/WAF-D-13-00061.1 , 2014. Thompson, G., Field, P. R., Rasmussen, R. M., & Hall, W. D.: Explicit forecasts of winter precipitation using an improved bulk microphysics scheme. Part II: Implementation of a new snow parameterization. <i>Monthly Weather Review</i> , 136(12), 5095-5115. https://doi.org/10.1175/2008MWR2387.1 , 2008. Wang, M., & Ullrich, P.: Marine air penetration in California's Central Valley: Meteorological drivers and the impact of climate change. <i>Journal of Applied Meteorology and Climatology</i> , 57(1), 137-154. https://doi.org/10.1175/JAMC-D-17-0089.1 , 2018. Wang, Y., Leung, L. R., Mcgregor, J. L., Lee, D. K., Wang, W. C., Ding, Y., & Kimura, F.: Regional climate modeling: progress, challenges, and prospects. <i>Journal of the</i>	<div style="border: 1px solid black; padding: 2px; margin-bottom: 5px;">Deleted: . (2008):</div> <div style="border: 1px solid black; padding: 2px; margin-bottom: 5px;">Deleted: ., ... &</div> <div style="border: 1px solid black; padding: 2px; margin-bottom: 5px;">Moved up [7]: Lauritzen, P.</div> <div style="border: 1px solid black; padding: 2px; margin-bottom: 5px;">Deleted: H. (2015):</div> <div style="border: 1px solid black; padding: 2px; margin-bottom: 5px;">Deleted: . (2016):</div> <div style="border: 1px solid black; padding: 2px; margin-bottom: 5px;">Deleted: . (2011):</div> <div style="border: 1px solid black; padding: 2px; margin-bottom: 5px;">Deleted: . (2008):</div> <div style="border: 1px solid black; padding: 2px; margin-bottom: 5px;">Deleted: . (2012):</div> <div style="border: 1px solid black; padding: 2px; margin-bottom: 5px;">Deleted: . (2014):</div> <div style="border: 1px solid black; padding: 2px; margin-bottom: 5px;">Deleted: . (2008):</div> <div style="border: 1px solid black; padding: 2px;">Deleted: . (2004):</div>
--	--	---

1252 Meteorological Society of Japan. Ser. II, 82(6), 1599-1628.
 1253 <https://doi.org/10.2151/jmsj.82.1599>, 2004.
 1254 Wicker, L. J., & Skamarock, W. C.: Time-splitting methods for elastic models using forward
 1255 time schemes. Monthly weather review, 130(8), 2088-2097.
 1256 [https://doi.org/10.1175/1520-0493\(2002\)130<2088:TSMFEM>2.0.CO;2](https://doi.org/10.1175/1520-0493(2002)130<2088:TSMFEM>2.0.CO;2), 2002.
 1257 Wu, C., Liu, X., Lin, Z., Rhoades, A. M., Ullrich, P. A., Zarzycki, C. M., ... & Rahimi-Esfarjani,
 1258 S. R.: Exploring a variable-resolution approach for simulating regional climate in the
 1259 Rocky Mountain region using the VR-CESM. Journal of Geophysical Research:
 1260 Atmospheres, 122(20), 10-939. <https://doi.org/10.1002/2017JD027008>, 2017.
 1261 Xiang, S., Li, Y., Li, D., & Yang, S.: An analysis of heavy precipitation caused by a retracing
 1262 plateau vortex based on TRMM data. Meteorology and Atmospheric Physics, 122(1-2),
 1263 33-45. <https://doi.org/10.1007/s00703-013-0269-1>, 2013.
 1264 Xu, H., & Yao, W.: A numerical study of the Beijing extreme rainfall of 21 July 2012 and the
 1265 impact of topography. Advances in Meteorology, 2015.
 1266 <http://dx.doi.org/10.1155/2015/980747>, 2015.
 1267 Xue, M., Kong, F., Weber, D., Thomas, K. W., Wang, Y., Brewster, K., ... & Coniglio, M. C.:
 1268 CAPS realtime storm-scale ensemble and high-resolution forecasts as part of the
 1269 NOAA Hazardous Weather Testbed 2007 spring experiment. In 22nd Conf. Wea. Anal.
 1270 Forecasting/18th Conf. Num. Wea. Pred, 2007.
 1271 Xu, Z., Rhoades, A. M., Johansen, H., Ullrich, P. A., & Collins, W. D.: An intercomparison of
 1272 GCM and RCM dynamical downscaling for characterizing the hydroclimatology of
 1273 California and Nevada. Journal of Hydrometeorology, 19(9), 1485-1506.
 1274 <https://doi.org/10.1175/JHM-D-17-0181.1>, 2018.
 1275 Yang, Q., Leung, L. R., Rauscher, S. A., Ringler, T. D., & Taylor, M. A.: Atmospheric moisture
 1276 budget and spatial resolution dependence of precipitation extremes in aquaplanet
 1277 simulations. Journal of Climate, 27(10), 3565-3581. <https://doi.org/10.1175/JCLI-D-13-00468.1>, 2014.
 1278
 1279 Yang, Q., R. Houze, Jr., L.R. Leung, & Z. Feng : Environments of long-lived mesoscale
 1280 convective systems over the Central United States in convection permitting climate
 1281 simulations. J. Geophys. Res., 122, <https://doi.org/10.1002/2017JD027033>, 2017.
 1282 Yao, X. P., Sun, J. Y., & Ma J. L.: Advances on research of Yangtze-Huaihe shear line. Plateau
 1283 Meteorology, 36(4), 1138-1151 (in Chinese), 2017.

Deleted: <https://doi.org/10.2151/jmsj.82.1599>

Deleted: . (2002):

Deleted: [https://doi.org/10.1175/1520-0493\(2002\)130<2088:TSMFEM>2.0.CO;2](https://doi.org/10.1175/1520-0493(2002)130<2088:TSMFEM>2.0.CO;2)

Deleted: . (2015):

Deleted: <http://dx.doi.org/10.1155/2015/980747>.

Deleted: . (2014):

Deleted: <https://doi.org/10.1175/JCLI-D-13-00468.1>

Deleted: (2017)

Deleted: Res., 122, doi: 10.1002/2017JD027033.

1294 1295 1296 1297 1298 1299 1300 1301 1302 1303 1304 1305 1306 1307 1308 1309 1310 1311 1312 1313 1314 1315 1316 1317 1318 1319 1320 1321 1322 1323 1324 1325 1326	Yessad, K., & Bénard, P.: Introduction of a local mapping factor in the spectral part of the Météo-France global variable mesh numerical forecast model. Quarterly Journal of the Royal Meteorological Society, 122(535), 1701-1719. https://doi.org/10.1002/qj.49712253511 , 1996. Zarzycki, C. M., Jablonowski, C., & Taylor, M. A.: Using variable resolution meshes to model tropical cyclones in the community atmosphere model. Monthly Weather Review, 142(3), 1221–1239. https://doi.org/10.1175/MWR-D-13-00179.1 , 2014. Zarzycki CM, Jablonowski C, Thatcher DR, Taylor MA: Effects of localized grid refinement on the general circulation and climatology in the community atmosphere model. J Clim 28:2777–2803. https://doi.org/10.1175/JCLI-D-14-00599.1 , 2015. Zhang, D. L., Lin, Y., Zhao, P., Yu, X., Wang, S., Kang, H., & Ding, Y.: The Beijing extreme rainfall of 21 July 2012: “Right results” but for wrong reasons. Geophysical Research Letters, 40(7), 1426-1431. https://doi.org/10.1002/grl.50304 , 2013. Zhang, H., & Zhai, P.: Temporal and spatial characteristics of extreme hourly precipitation over eastern China in the warm season. Advances in atmospheric sciences, 28(5), 1177. https://doi.org/10.1007/s00376-011-0020-0 , 2011. Zhang, L., Dong, M., & Wu, T.: Changes in precipitation extremes over eastern China simulated by the Beijing Climate Center Climate System Model (BCC_CSM1. 0). Climate Research, 50(2-3), 227-245. https://doi.org/10.3354/cr01066 , 2011. Zhang, Q., Xiao, M., Singh, V. P., Liu, L., & Xu, C. Y.: Observational evidence of summer precipitation deficit-temperature coupling in China. Journal of Geophysical Research: Atmospheres, 120(19). https://doi.org/10.1002/2015JD023830 , 2011. Zhang, Q., Zheng, Y., Singh, V. P., Luo, M., & Xie, Z.: Summer extreme precipitation in eastern China: Mechanisms and impacts. Journal of Geophysical Research: Atmospheres, 122(5), 2766-2778. https://doi.org/10.1002/2016JD025913 , 2017. Zhang, Y., P., L., & Zhong, Q.: An interdecadal change in the relationship between the western North Pacific Ocean and the East Asian summer monsoon. Climate Dynamics, 49(4), 1139-1156. https://doi.org/10.1007/s00382-016-3370-6 , 2017. Zhai, P., Zhang, X., Wan, H., & Pan, X.: Trends in total precipitation and frequency of daily precipitation extremes over China. Journal of Climate, 18(7), 1096-1108. https://doi.org/10.1175/JCLI-3318.1 , 2005. Zhao, C., Leung, L. R., Park, S. H., Hagos, S., Lu, J., Sakaguchi, K., ... & Duda, M. G.: Exploring the impacts of physics and resolution on aqua,planet simulations from a	<div style="border: 1px solid black; padding: 2px; margin-bottom: 5px;">Deleted: . (1996):</div> <div style="border: 1px solid black; padding: 2px; margin-bottom: 5px;">Deleted: https://doi.org/10.1002/qj.49712253511</div> <div style="border: 1px solid black; padding: 2px; margin-bottom: 5px;">Deleted: Levy, M. N.,</div> <div style="border: 1px solid black; padding: 2px; margin-bottom: 5px;">Deleted: Overfelt, J. R.,</div> <div style="border: 1px solid black; padding: 2px; margin-bottom: 5px;">Deleted: ., &</div> <div style="border: 1px solid black; padding: 2px; margin-bottom: 5px;">Moved up [8]: Ullrich, P.</div> <div style="border: 1px solid black; padding: 2px; margin-bottom: 5px;">Deleted: A. (2014): Aquaplanet experiments using CAM’s</div> <div style="border: 1px solid black; padding: 2px; margin-bottom: 5px;">Deleted: -</div> <div style="border: 1px solid black; padding: 2px; margin-bottom: 5px;">Deleted: dynamical core. Journal</div> <div style="border: 1px solid black; padding: 2px; margin-bottom: 5px;">Deleted: Climate, 27(14), 5481-5503.</div> <div style="border: 1px solid black; padding: 2px; margin-bottom: 5px;">Deleted: https://doi.org/10.1175/JCLI-D-14-00004.1</div> <div style="border: 1px solid black; padding: 2px; margin-bottom: 5px;">Deleted: . (2013):</div> <div style="border: 1px solid black; padding: 2px; margin-bottom: 5px;">Deleted: https://doi.org/10.1002/grl.50304</div> <div style="border: 1px solid black; padding: 2px; margin-bottom: 5px;">Deleted: . (2011):</div> <div style="border: 1px solid black; padding: 2px; margin-bottom: 5px;">Deleted: https://doi.org/10.1007/s00376-011-0020-0</div> <div style="border: 1px solid black; padding: 2px; margin-bottom: 5px;">Deleted: . (2011):</div> <div style="border: 1px solid black; padding: 2px; margin-bottom: 5px;">Deleted: https://doi.org/10.3354/cr01066</div> <div style="border: 1px solid black; padding: 2px; margin-bottom: 5px;">Deleted: . (2015):</div> <div style="border: 1px solid black; padding: 2px; margin-bottom: 5px;">Deleted: https://doi.org/10.1002/2015JD023830</div> <div style="border: 1px solid black; padding: 2px; margin-bottom: 5px;">Deleted: . (2017):</div> <div style="border: 1px solid black; padding: 2px; margin-bottom: 5px;">Deleted: https://doi.org/10.1002/2016JD025913</div> <div style="border: 1px solid black; padding: 2px; margin-bottom: 5px;">Deleted: . (2017):</div> <div style="border: 1px solid black; padding: 2px; margin-bottom: 5px;">Deleted: https://doi.org/10.1007/s00382-016-3370-6.</div> <div style="border: 1px solid black; padding: 2px; margin-bottom: 5px;">Deleted: . (2005):</div> <div style="border: 1px solid black; padding: 2px; margin-bottom: 5px;">Deleted: . (2016):</div>
--	--	---

1352	nonhydrostatic global variable-resolution modeling framework. Journal of Advances	Deleted: variable-resolution
1353	in Modeling Earth Systems, 8(4), 1751-1768. https://doi.org/10.1002/2016MS000727 ,	Deleted: https://doi.org/10.1002/2016MS000727
1354	2017 .	
1355	Zhao, Y., Xu, X., Zhao, T., Xu, H., Mao, F., Sun, H., & Wang, Y.: Extreme precipitation events	Deleted: . (2016):
1356	in East China and associated moisture transport pathways. Science China Earth	
1357	Sciences, 59(9), 1854-1872. https://doi.org/10.1007/s11430-016-5315-7 , 2016 .	Deleted: https://doi.org/10.1007/s11430-016-5315-7
1358	Zheng, Y., Xue, M., Li, B., Chen, J., & Tao, Z.: Spatial characteristics of extreme rainfall over	Deleted: . (2016):
1359	China with hourly through 24-hour accumulation periods based on national-level	
1360	hourly rain gauge data. Advances in Atmospheric Sciences, 33(11), 1218-1232.	
1361	https://doi.org/10.1007/s00376-016-6128-5 , 2016 .	Deleted: https://doi.org/10.1007/s00376-016-6128-5
1362	Zhong, S., pQian, Y., Zhao, C., Leung, R., & Yang, X. Q.: A case study of urbanization impact	Deleted: . (2015):
1363	on summer preciitation in the Greater Beijing Metropolitan Area: Urban heat island	
1364	versus aerosol effects. Journal of Geophysical Research: Atmospheres, 120(20), 10-	
1365	903. https://doi.org/10.1002/2015JD023753 , 2015 .	Deleted: https://doi.org/10.1002/2015JD023753
1366	Zhong, S., Qian, Y., Zhao, C., Leung, R., Wang, H., Yang, B., ... & Liu, D.: Urbanization-	Deleted: . (2017):
1367	induced urban heat island and aerosol effects on climate extremes in the Yangtze River	
1368	Delta region of China. Atmospheric Chemistry and Physics, 17(8), 5439-5457.	
1369	https://doi.org/10.5194/acp-17-5439-2017 , 2017 .	Deleted: https://doi.org/10.5194/acp-17-5439-2017
1370	Zhou, T. J., & Li, Z.: Simulation of the East Asian summer monsoon using a variable resolution	Deleted: . (2002):
1371	atmospheric GCM. Climate Dynamics, 19(2), 167-180.	
1372	https://doi.org/10.1007/s00382-001-0214-8 , 2002 .	Deleted: https://doi.org/10.1007/s00382-001-0214-8
1373		
1374		
1375	▼	Deleted: .

1389
1390
1391
1392
1393

1394
1395
1396
1397
1398
1399
1400
1401
1402
1403

1404
1405
1406
1407
1408

Table 1 Numerical Experiments conducted and analyzed in this study

Physics/Resolution	MPAS				
	U15km	U60km	V30km	V16km	V4km
WSM6+NTD	Yes	/	/	Yes	/
WSM6+GF	Yes	Yes	Yes	Yes	Yes
Thompson+GF	/	/	/	/	Yes

(1) ‘U’ and ‘V’ represent quasi-uniform and variable resolution meshes, respectively, as described in the Section 2.1.2.
(2) ‘WSM6’ and ‘Thompson’ represent two cloud microphysics schemes as described in the Section 2.1.1; ‘NTD’ and ‘GF’ represent two cumulus parameterizations as described in the Section 2.1.1.

Table 2 The correlation coefficients and the corresponding 95% confidence intervals based on the bootstrap analysis for the results shown in Fig. 6-10

	GFS.1deg	GFS.0.5deg	U60km.WSM6	V30km.WSM6	V16km.WSM6	V4km.WSM6	V4km.Thompson
Fig. 6	0.06 (0.006~0.1)	0.03 (-0.01~0.08)	0.49 (0.45~0.54)	0.47 (0.43~0.53)	0.56 (0.50~0.61)	0.63 (0.54~0.67)	0.54 (0.48~0.59)
Fig. 7	-0.15 (-0.35~0.24)	-0.19 (-0.39~0.15)	0.68 (0.49~0.84)	0.71 (0.46~0.88)	0.89 (0.78~0.95)	0.97 (0.93~0.99)	0.72 (0.45~0.93)
Fig. 8	0.03 (-0.02~0.09)	0.02 (-0.03~0.08)	0.30 (0.25~0.37)	0.32 (0.27~0.41)	0.41 (0.37~0.48)	0.42 (0.39~0.49)	0.38 (0.32~0.44)
Fig. 9	0.32 (0.23~0.41)	0.29 (0.20~0.41)	0.53 (0.45~0.61)	0.68 (0.64~0.72)	0.80 (0.77~0.83)	0.85 (0.82~0.88)	0.80 (0.75~0.84)
Fig. 10	L	L	0.20 (0.13~0.28)	0.21 (0.12~0.30)	0.30 (0.19~0.40)	0.50 (0.39~0.59)	0.42 (0.34~0.51)

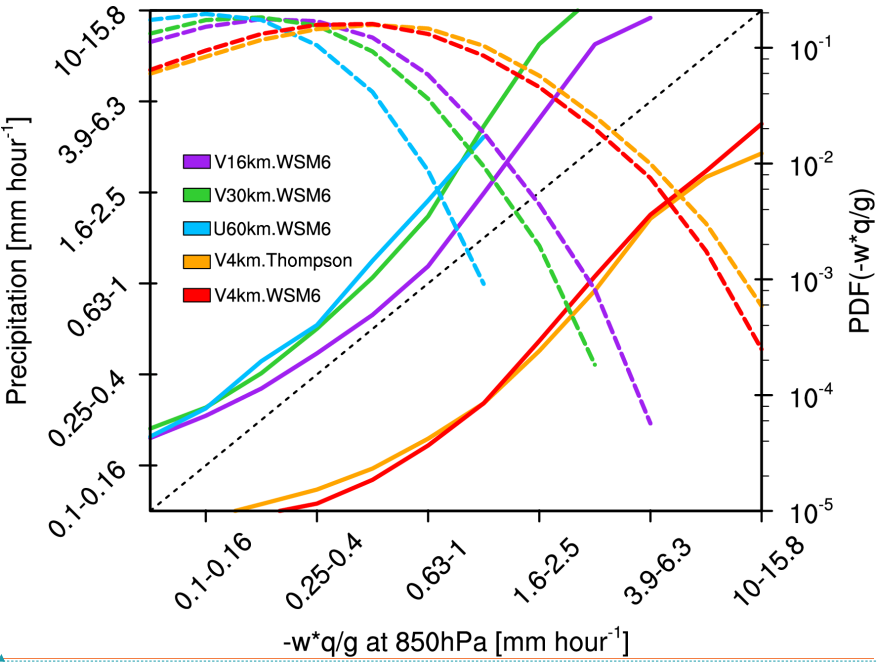
(1) The values inside the parenthesis indicate the lower and higher bounds of 95% confidence intervals; the values outside are estimated directly based on the results shown in Fig. 6-10.

Formatted: Font:Times New Roman
Formatted: Justified

Deleted: ... [2]

Formatted: Left, Line spacing: single, Tabs: 8.19 cm, Left

1411
1412
1413
1414
1415



1416
1417
1418
1419
1420
1421
1422

Figure 13 Hourly precipitation versus upward moisture flux at 850hPa during the event over East China from the MPAS simulations at the resolution of 60km, 30km, 16km and 4km (solid line, left axis), and the PDFs of the upward moisture flux (dash line, right axis).

Formatted: Font:(Default) Times New Roman

& McGregor, J. L. (2006): Variable resolution general circulation models: Stretched grid model intercomparison project (SGMIP). Journal of Geophysical Research: Atmospheres, 111(D16). <https://doi.org/10.1029/2005JD006520>

Fox-Rabinovitz, M. S., Stenchikov, G. L., Suarez, M.